Chapter 11

Environmental Application of High Sensitive Gas Sensors with Tunable Diode Laser Absorption Spectroscopy

Xiaojuan Cui, Fengzhong Dong, Zhirong Zhang, Hua Xia, Tao Pang, Pengshuai Sun, Bian Wu, Shuo Liu, Luo Han, Zhe Li and Runqing Yu

Additional information is available at the end of the chapter

http://dx.doi.org/10.5772/intechopen.72948

Abstract

Due to the fact of global warming, air quality deterioration and health concern over the past few decades, great demands and tremendous efforts for new technology to detect hazard gases such as CH_4, CO_2, CO, H_2S, and HONO have been performed. Tunable diode laser absorption spectroscopy (TDLAS) is a kind of technology with advantages of high sensitivity, high selectivity, and fast responsivity. It has been widely used in the applications of greenhouse gas measurements, industrial process control, combustion gas measurements, medicine, and so on. In this chapter, we will briefly summarize the most recent progress on TDLAS technology and present several kinds of gas sensors developed mainly by our group for various field applications. These could expand from energy, environment, and public safety to medical science.

Keywords: TDLAS, wavelength modulation, hazard gases, HONO, $\delta^{13}C$

1. Introduction

Over the past few decades, environmental pollution problem has occurred to different degrees in the whole world, such as atmospheric pollution, marine pollution, and urban environmental problems. With the globalization of economy and trade, environmental pollution is becoming more and more internationalized [1]. In order to control environmental pollution, great demands and tremendous efforts for new technology to detect hazard gases such as CH_4,

CO_2, CO, HONO, H_2S, and HCl have been performed. This would be beneficial for the implementation of global environmental protection policies for the reduction of gas pollution and for a general environmental management [2].

Several optical techniques have been developed to detect these hazard gases in the atmosphere [3–10]. Cavity-enhanced spectroscopy (CEAS) or cavity ring-down spectroscopy (CRDS) has been demonstrated to enable measurements of multiple gases with a low detection limit of sub-ppb [4–6]. However, these two technologies require critical optical alignment and regular cleaning of mirrors of the external cavity which affects continuous monitoring of atmospheric species in the field. Quartz-enhanced photoacoustic spectroscopy (QEPAS) technique was also developed for environmental and biomedical measurements [7, 8]. Nevertheless, the high modulation frequencies used in QEPAS may represent a problem for multicomponent gas mixtures containing varying amounts of water vapor such as ambient air, due to the strong influence of water vapor on the molecular vibrational-translational (V-T) relaxation times. Other spectroscopic methods such as open path Fourier transform infrared spectrometry (FTIR) and differential optical absorption spectroscopy (DOAS) have been reported for atmospheric molecule detection [9, 10]. But the minimum detection limits (MDLs) of FTIR usually exceed the requirements for high sensitivity measurements of the atmospheric species. The main disadvantage of the DOAS system is that its spatial resolution is rather poor with a path length generally greater than 1 km.

The technique based on tunable diode laser absorption spectroscopy (TDLAS) is an effective method to measure gas mixing ratios and multiple parameters with high selectivity, high sensitivity, high precision, and high response time [11–18]. Especially, with the development of multi-pass absorption cells, the effective optical path length can be extended from a few meters to several hundred meters; the sensitivity is significantly improved [19–21]. In order to further improve the signal-to-noise ratio (SNR), the wavelength modulation spectroscopy (WMS) technology with second harmonic (2f) signals is usually employed in the TDLAS system to measure the gas concentration.

The first commercial TDLAS gas sensor was introduced on the market in 1995 using the trademark laser gas by Norsk Elektro Optikk Company. Over the past decades, TDLAS has been extensively investigated potentially as an effective method to measure multiple gas parameters and is widely used in various areas such as gas mixing ratio detection, vehicle emissions, gas exhaust temperature monitoring, carbon isotope measurements, and so on [22–37]. Now NEO Monitors is one of the world leading suppliers of the TDLAS-based gas analyzers and dust monitors. Its products are widely used in the field of industrial process control and emission monitoring; nearly 6000 sets of laser gas analyzers were installed in more than 40 countries and regions in the world currently. We are also developing instruments based on TDLAS technology to satisfy the needs of environmental monitoring and industrial process control in China. **Figure 1** shows several pictures of the gas sensors developed by our research team. In this chapter, we will briefly present several kinds of gas sensors developed by our research group for various field applications, which could expand from environment and public safety to medical science.

http://dx.doi.org/10.5772/intechopen.72948

Figure 1. Several pictures of the TDLAS system developed by our research team.

2. Basic principles of TDLAS

Based on the Beer-Lambert law, the relationship between the incident intensity I_0 and the transmitted intensity I can be expressed as

$$I = I_0 \exp(-kL) \tag{1}$$

where k is the absorption coefficient and L denotes the path length (in cm). In the near-infrared region, the gas absorption coefficient is usually very small, i.e., $kL \leq 0.05$ [38]. Eq. (1) can thus be simplified as

$$I = I_0(1 - kL) = I_0[1 - \sigma(\nu)CL] \tag{2}$$

where σ(ν) is the absorption cross section (in [cm^2/molecule]) at frequency ν and C is the gas mixing ratio. The integrated absorbance A_I (in [cm^{-1}]) can be written as

$$A_I = \int A(\nu)d\nu = \int \ln(I_0(\nu)/I(\nu))d\nu = \mathrm{NL}\int \sigma(\nu)d\nu = \mathrm{NLS} \tag{3}$$

N is the number of absorbing molecules (in [molecules/cm^3]); S is the molecule absorption line strength (in [cm^2/(mol cm)]). Based on Eq. (3), the gas species mixing ratio can be retrieved from the integrated absorbance A_I measured at temperature T and pressure P [39]:

$$C(\mathrm{ppm}) = \frac{N}{N_T} \times 10^6 = \frac{A_I P_0 T}{N_L \mathrm{P T_0 LS}} \times 10^6 \tag{4}$$

where N_L = 2.6868 × 10^{19} mol/cm^3 represents the Loschmidt number at T_0 = 273.15 K and P_0 = 760 Torr.

For gas mixing ratio detection, WMS is often adopted. The intensity of 2f signal can be expressed as [40]

$$I_{2f} \propto I_0 \sigma_0 CL \tag{5}$$

When the reference signal and nonlinear least square multiplication method are introduced to fit the 2f signals of the target gas [41], Eq. (5) can be rewritten as

$$C_{Mea} = a\frac{I_{Mea} C_{\mathrm{Ref}} L_{\mathrm{Ref}}}{I_{\mathrm{Ref}} L_{Mea}} \tag{6}$$

where a is fitting coefficient; C_{Mea} and C_{Ref} are the mixing ratios of the target gas to be measured and reference gas in the calibration cell, respectively; I_{Ref} and I_{Mea} denote the intensities of the two split laser beams; and L_{Ref} and L_{Mea} represent the calibration cell and the measurement optical path length, respectively. In general, the ratio of the 2f and 1f signals can be used to cancel any laser intensity differences. In this case, the mixing ratio from the following equation could be easily obtained:

$$C_{Mea} = \frac{\left(\frac{I_{2f}}{I_{1f}}\right)_{Mea} C_{\mathrm{Ref}} L_{\mathrm{Ref}}}{\left(\frac{I_{2f}}{I_{1f}} 1f\right)_{\mathrm{Ref}} L_{Mea}} \tag{7}$$

where $\left(\frac{I_{2f}}{I_{1f}}\right)_{\mathrm{Ref}}$ and $\left(\frac{I_{2f}}{I_{1f}}\right)_{Mea}$ represent the 2f/1f ratio value of the reference and target gas signals, respectively.

3. Methane (CH_4) monitoring

3.1. Introduction

With the increasing attention to environment, energy, and safety, natural gas has gradually replaced coal as the main energy source in China, and its use has been increasing year by year.

The extraction, transportation, and storage of natural gas have become an important part of social development. Equipment safety and high efficiency operation in gas transmission station are the keys to ensure the natural gas transportation. Once it is released, the serious safety accidents such as energy waste, environmental pollution, fire, and explosion will happen [42], which would directly threaten the safety of life and property of the countries and people [43].

The main component of natural gas is methane, accounting for 90%, and also contains a small amount of ethane, acetylene, butane, carbon dioxide, carbon monoxide, hydrogen sulfide, and so on. Traditional natural gas leakage detectors include flame ion detectors (FID), electronic detectors, electrochemical catalytic combustion detectors, and infrared absorption detectors [44]. However, these detectors are self-charging and have potential safety problems in the application of flammable, explosive, and other special environments. Moreover, these sensors are short in life, low in precision, poor in stability, and difficult in adjustment and often give the wrong results of measurements and misinformation. Recently, TDLAS technology has been widely used with the rapid development of narrow linewidth semiconductor laser technology [45]. The SRI International (Menlo Park, CA) company in America has developed a vehicular natural gas pipeline leakage detector, which improves the efficiency of pipeline leakage detection. However, they are all limited to the detection of methane and do not involve the detection of other gases in natural gas.

In view of the area of natural gas, gathering station is large, and the pipeline system of natural gas is gathered; point and portable measurement is not suitable in this situation. We designed an open, continuous detection and alarm system which has the characteristics of fast response speed and high detection precision based on TDLAS technology. Moreover, this system also detects ethylene, acetylene, and other gases, which improves the measurement precision and reduces the probability of false alarm.

3.2. Absorption line selection

The near-infrared absorption band matches with the low loss window of optical fiber and is convenient for long-distance transmission and multipoint distributed detection by using fiber and fiber devices. Therefore, the absorption lines of selected CH_4, C_2H_2, and C_2H_4 are 1653.72, 1531.59, and 1621.36 nm, respectively. There are three adjacent absorption lines at 1653.72 nm for CH_4, which are close to each other and cannot be separated in the atmospheric pressure by consulting the HITRAN 2008 database. In the experiment, they are processed as one absorption line. The C_2H_4 absorption lines are not included in HITRAN database. A large amount of absorption lines of C_2H_4 from 1600 to 1650 nm can be found from the PNNL25C (Northwest Pacific National Laboratory) database which have been already experimentally verified in the literature [46]. The parameters of three gases absorption lines are shown in **Table 1**.

3.3. DFB-based experimental platform

The system is designed mainly aimed at the gas gathering station, and the schematic diagram of the system is shown in **Figure 2**. Three butterfly-packaged distributed feedback (DFB) lasers are selected to detect CH_4, C_2H_2, and C_2H_4 with the center output wavelengths of 1653, 1531, and 1621 nm, respectively. The light sources are controlled by the corresponding temperature,

Molecule	Wavenumber (nm)	Line strength at 300 K (cm^{-2} atm^{-1})	Δν (cm^{-1})
CH_4	1653.7282	0.0206	0.14
	1653.7256	0.0206	
	1653.7225	0.0368	
C_2H_2	1531.5878	0.2916	0.23
C_2H_4	1621.3600		

Table 1. The parameters of absorption lines.

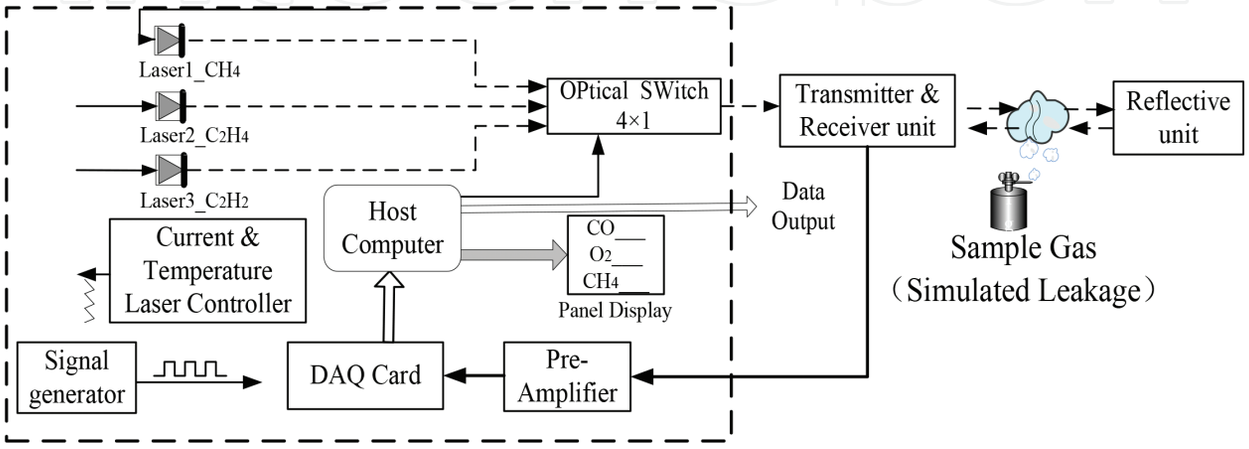

Figure 2. Schematic diagram of the experimental system.

current driver module, and signal generator module, respectively. Three modulation light beams are time-sharing output through a 3 × 1 optical switch which is controlled by a microprocessor and then the collimator and beam expander of the transmitter (THORLABS GBE10-C: ten times beam expander, 1050–1650 nm antireflective coating), passing through the measurement area to the corner cube mirror at the reflecting end. Then, returning to the receiving end along the parallel light path, the light beam containing the absorption signal is focused on the photosensitive surface of the photoelectric detector through an aspherical focusing lens and converted into electrical signals before entering the host control section. The amplified electrical signals are collected by the data acquisition card and transmitted to the microprocessor system after amplification by the preamplifier circuit. Finally, the online inversion of spectral data is carried out to obtain the gas concentration. Meanwhile, the early warning will be carried out according to the setting of the alarm limit. If the value exceeds the setting one; the system will send out light and sound alerting signal.

In order to decide the detection limit of the system, a calibration experiment was designed and shown in **Figure 3**. A calibrated absorption cell with a length of 1 m was placed on the laser path. In the calibration experiment, three gases CH_4, C_2H_2, and C_2H_4 with the mixing ratios of 1%, 500, and 500 ppm are mixed in the absorption cell, and the corresponding absorption signals are displayed in **Figure 4**. The absorption lines of CH_4 and C_2H_2 are independent, and there are no other spectral interferences, but there is a relatively weak absorption spectral line

http://dx.doi.org/10.5772/intechopen.72948

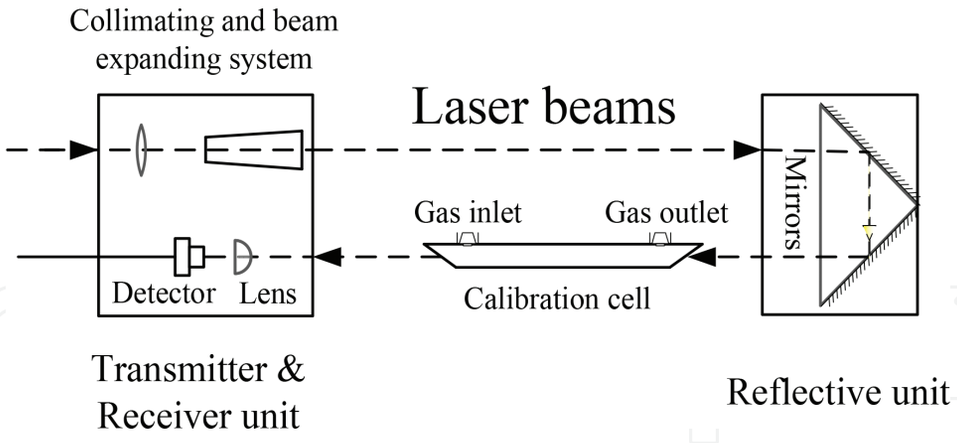

Figure 3. Schematic diagram of calibration principle.

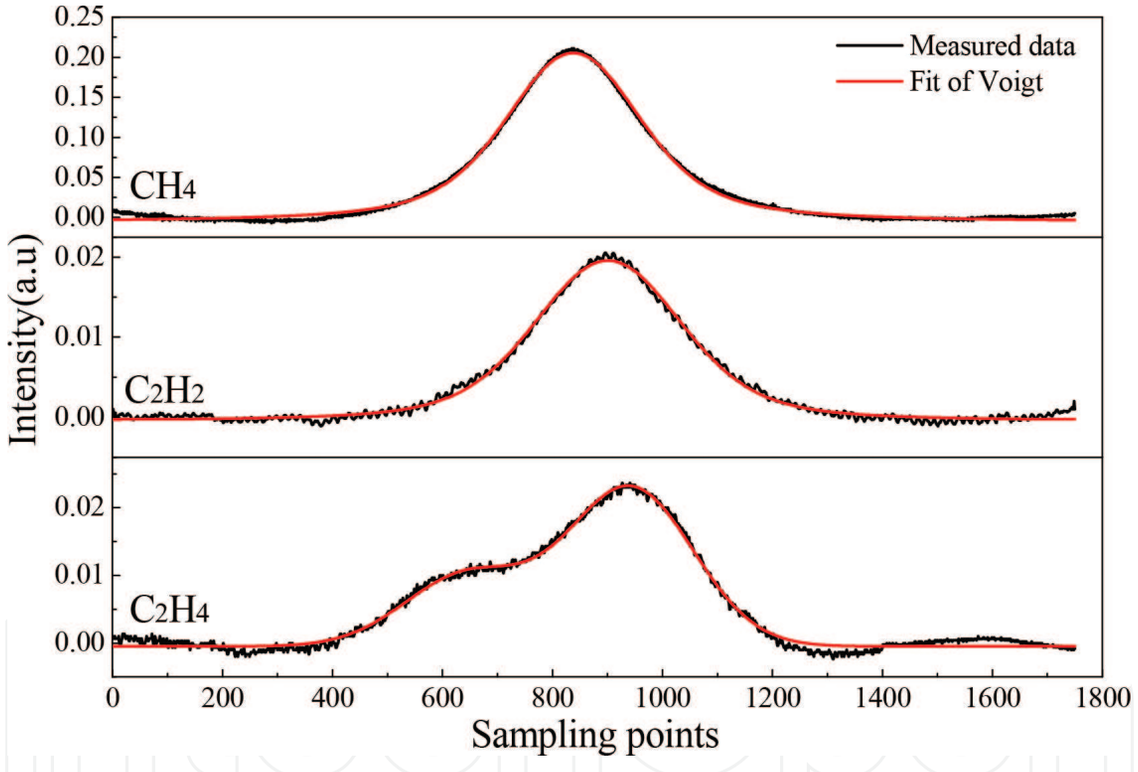

Figure 4. Direct absorption signal and fitting results.

on the left of the absorption line of C_2H_4. Therefore, the absorption lines of CH_4 and C_2H_2 are fitted using a single peak, and the absorption line of C_2H_4 is fitted by double peak in the fitting process. The absorbance A values of CH_4, C_2H_2, and C_2H_4 absorption spectral lines are 0.076, 0.012, and 0.014 cm^{-1}, respectively. The SNR of the absorption signals are 100, 12, and 10, respectively. According to the linear relationship between the direct absorbance and gas concentration, the obtained MDLs of CH_4, C_2H_2, and C_2H_4 were 100, 40, and 50 ppm-m, respectively, which completely satisfied the gas gathering station leakage test requirements [47].

3.4. Results and discussion

The system had been field-tested at the testing ground of China Petroleum Pipeline Bureau. The environment temperature was 35°C, air relative humidity was 45%, and wind speed was 1 m/s during the experiment. We used the gas which was mixed with 90% methane, 5% ethylene, and 5% acetylene to simulate gas pipeline leakage in the experiment. The leakage position was about 2 m below the side of the laser beam. In order to measure the three gases simultaneously, lasers were switched every 10 seconds using an optical switch. Three kinds of gases were detected circularly in the order of $CH_4 \rightarrow C_2H_2 \rightarrow C_2H_4$. The mixing ratios of the gases are exhausted 1 minute each time which was displayed in **Figure 5**. The reason for fluctuations is that the measured concentrations are the average of the paths along the line of sight. Due to the uncertainty of wind speed and gas diffusion in the measurement field, the concentration on the beam path fluctuates greatly. Meanwhile, this system is also equipped with an alarm limit for each gas, and the veracity of fire alarming system achieved 100%.

The system includes three DFB lasers which have an output power of about 20 mW higher than the other semiconductor lasers. Moreover, the optical fiber loss is less than 0.25 dB/km in this waveband. So the system can connect four pairs of transmitter and receiver units simultaneously. According to the requirements and distribution of gas pipeline, gas gathering device, housing, and other special places in the gas gathering station, the installation scheme including a host control machine and two pairs of transmitter and receiver units was designed and displayed in **Figure 6**. This system can be used to monitor the leakage of natural gas station in the range of 100 × 100 m.

The leakage detection system based on TDLAS can detect methane, ethylene, and acetylene rapidly and effectively in the open environment, and the response time of the three gases is less than 2 s. The accuracy of giving an alarm is 100%, which can be used in natural gas station and valve room gas leakage. Compared to other techniques, this technique has the advantages of safety in nature, no calibration, high accuracy, and little environmental effects. The MDLs for methane, acetylene, and ethylene gas are 100, 40, and 50 ppm-m, respectively, which meet the requirements for the detection of natural gas leakage in the petrochemical industry.

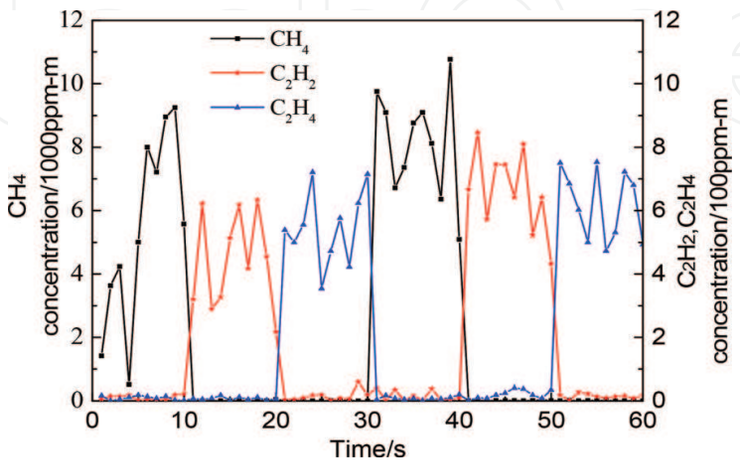

Figure 5. Concentration curves of experiment results.

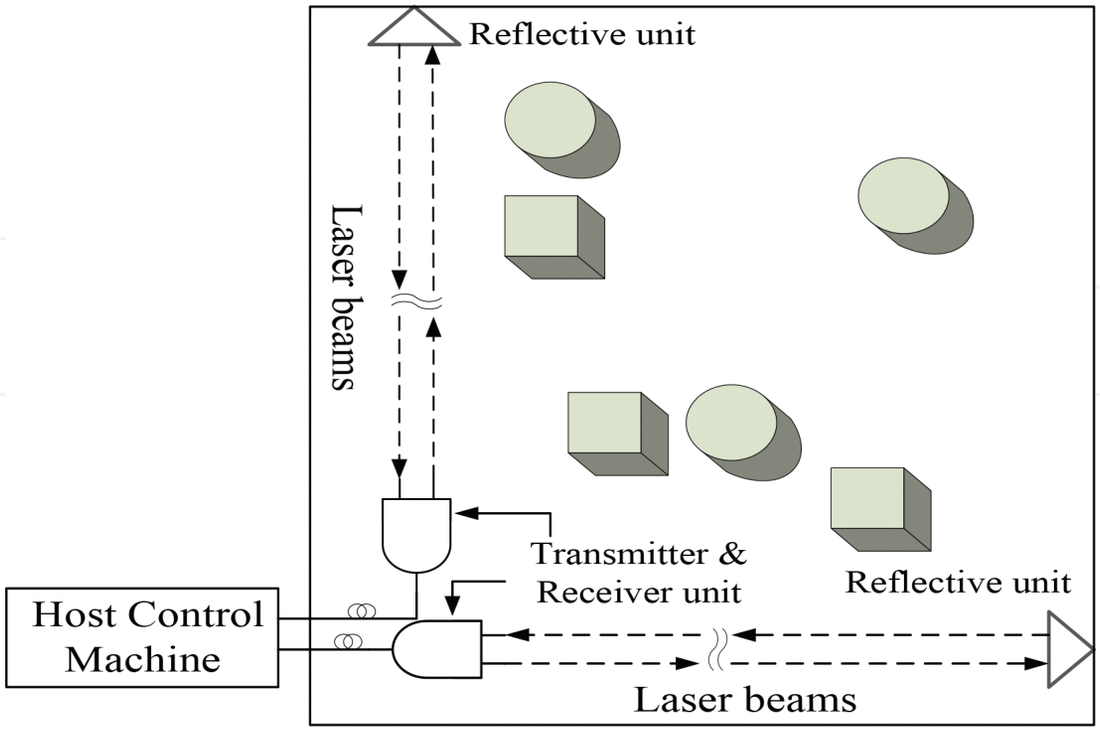

Figure 6. Installation scheme of natural gas gathering and transferring station.

4. Carbon monoxide (CO) monitoring

4.1. Introduction

CO is a kind of toxic, combustible, explosive gas and brings lots of hidden danger to the production and life of human beings. The research of coal spontaneous combustion suggests that a series of gases which could indicate the degree of oxidation and combustion of coal will be produced when coal seam is on fire. Using the relationship between the amount of indicator gases and the rate of change could predict coal seam fire at an early stage. Nowadays, CO is widely used as the main indicator gas for early warning of coal seam fire because the quantity of CO is closely related to the temperature of coal seam and the concentration change is obvious. In addition, the safety production under the mine has attracted much attention. In order to avoid accidents, gas monitoring has become a necessary means. The detection devices of the main gas constituents such as methane and carbon dioxide have been improved and widely used. With the improvement of security awareness, people have higher requirements on the accuracy of gas monitoring [48].

4.2. Absorption line selection

The absorption intensity of CO in the mid-infrared region is two orders of magnitude higher than that of overtone band in the near infrared. With the development of mid-infrared lasers, high sensitivity detection of CO has been obtained by some researchers [49]. But for the long-

distance optical fiber transmission signals, the use of the mid-infrared laser is limited because the current optical fiber communication windows are mainly concentrated in the near infrared. The intensity of CO absorption line in the near infrared is weak, and the SNR is poor when low concentration is detected, which requires higher stability of the measurement system. At present, the stability research of high sensitivity detection of CO in the near infrared has not been reported. But there are some reports about measurement techniques such as the stability of DFB lasers [50], the application of signal processing in CO_2 and NO_2, and other gas measurements [51]. Therefore, it is of great practical significance to study the stability of whole measurement system and realize the high sensitivity detection of CO in the communication windows.

To select a unique gas absorption line usually adopts the following guide rules: (1) strong absorption line strength with good line profile and (2) free of interference from other gases. The second overtone band near 1.566 μm of CO was selected in this work to avoid interferences from other major ambient gases in the mixture. **Figure 7** shows the absorption spectrum of CO, CO_2, and H_2O near the wavelength range of 1.566 μm [52].

4.3. Experimental system design

The experimental system is shown in **Figure 8**. The system adopts balanced optical path detection method. The 2 * 1 beam combiner couples the collimated light and the measuring beam to the 1*3 beam splitter, after that the first beam through a multi-pass absorption cell filled with CO gas, marked as S (measuring light path); the second beam through a high

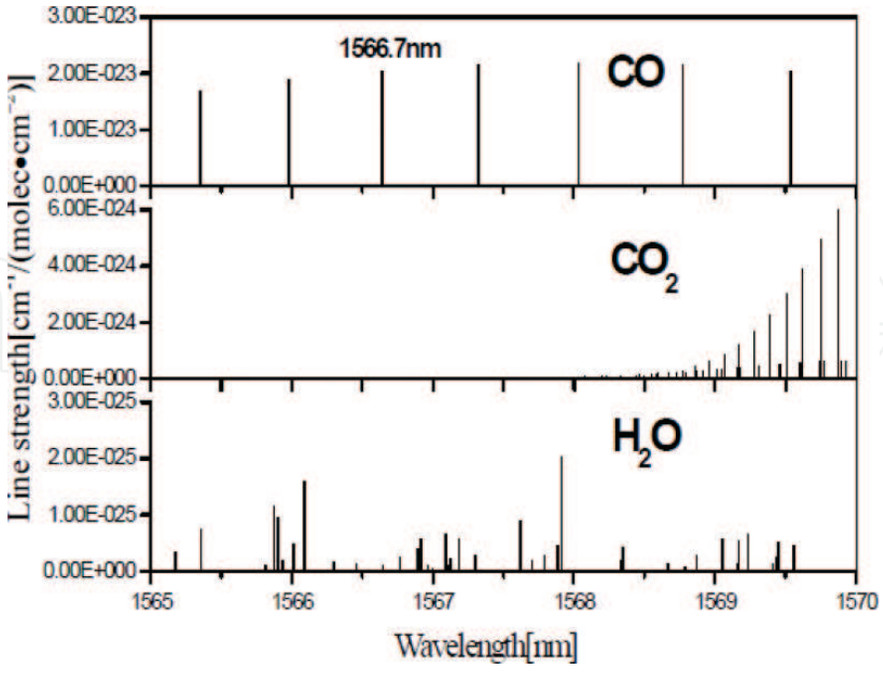

Figure 7. The absorption lines of CO, CO_2, and H_2O near the wavelength range of 1.566 μm (HITRAN 2008 database).

http://dx.doi.org/10.5772/intechopen.72948

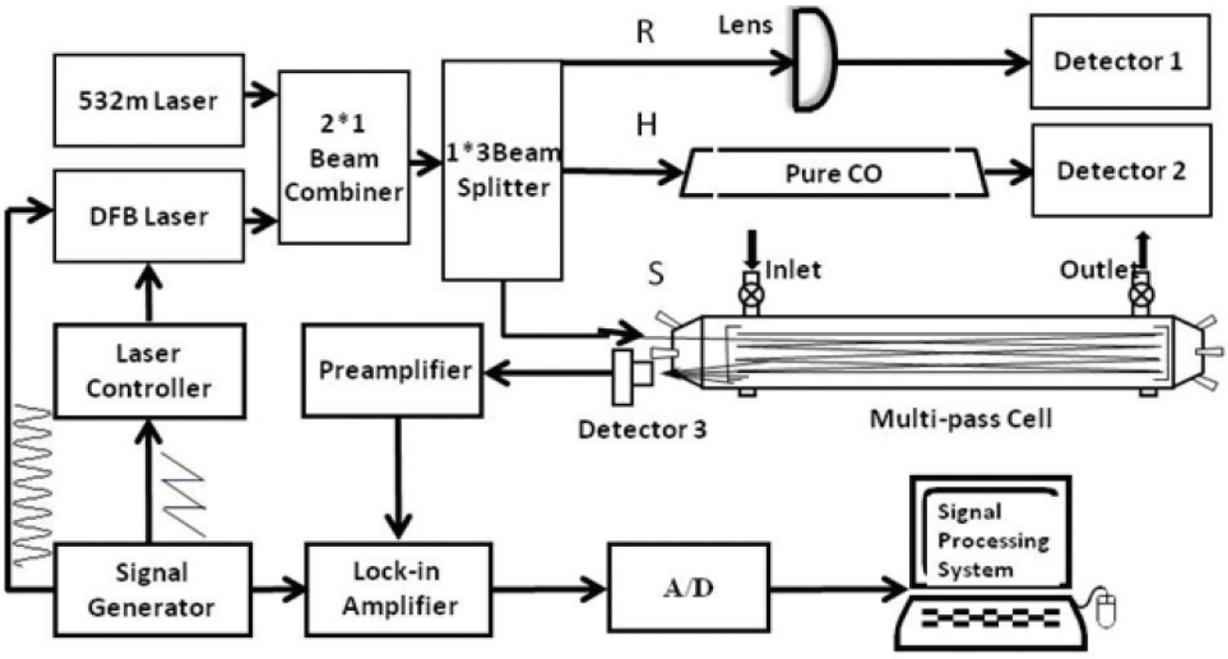

Figure 8. Schematic diagram of the TDLAS experimental system.

concentration reference cell with 100% CO, used to determine and control the position of absorption wavelength, marked as H; and the third beam is a reference light through the free space, used to monitor the changes of the laser background, marked as R. The three detection signals are sequential controlled by the switching circuit simultaneously. The wavelength is scanned with 100 Hz sawtooth wave and modulated with 10 kHz sine wave. More details about the electronics setup for the experiment could be found in [53]. Three modulation signals enter the lock-in amplifier through the switching circuit. In the lock-in amplifier, the detector output is mixed with the reference signal (10 kHz) to demodulate the 2f spectral signal. Then the 2f signal is simultaneously processed by a data acquisition card installed on a computer.

A new type of multi-pass absorption cell was developed and effectively improved the detection ability of the system. The new absorption cell has the advantages of simple structure, stable performance, effective use of the surface area, and solving the contradiction between the small volume and long-path length. The optical path length of 56.7 m was achieved in the volume of 1 L. At the same time, the optical path is adjustable; the spot array is uniform and in order, so that the optical path calculation is convenient; and the free spectral range is very narrow. The possible interference fringes in the cell are distributed in the high frequency region. By means of the digital averaging method, the influence of interference fringes on the second harmonic signals can be removed effectively and simply. The base length of the multi-pass absorption cell used in the system is 24.6 cm; the diameter of the mirror is 60 mm. According to the needs of TDLAS system for CO gas measurement, the mirror is coated with a dielectric film with a high reflectivity (typically 0.999) for wavelengths 532 and 1567 nm, wherein 532 nm is the collimated light during the alignment of the optical path. **Figure 9** shows the spot distribution of the mirrors at both ends of the absorption cell.

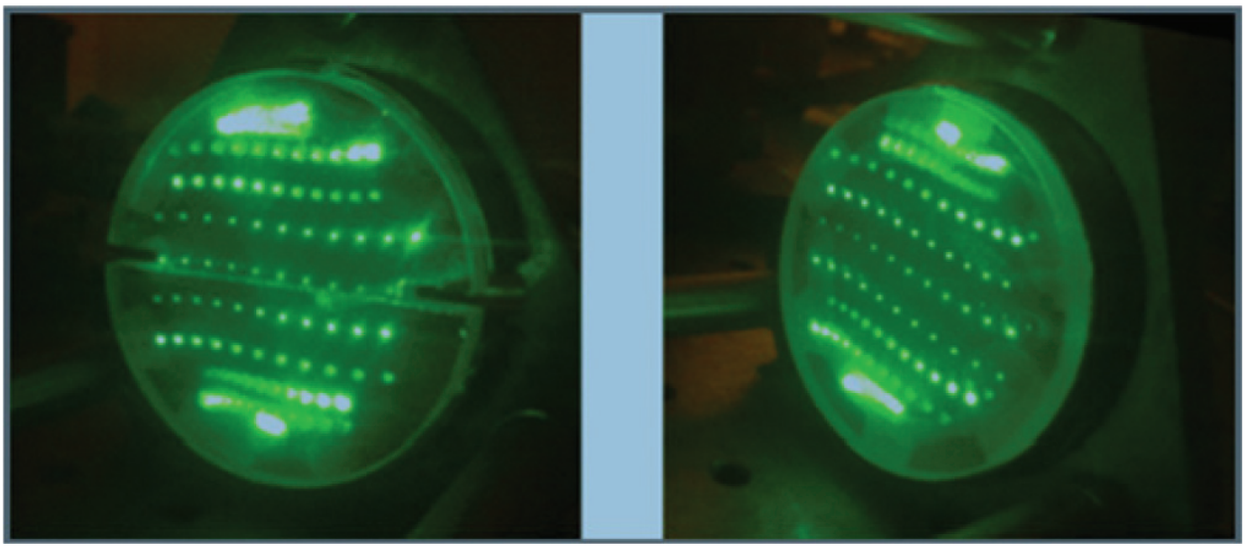

Figure 9. Light spot distribution of the mirrors at the both ends of the absorption cell.

4.4. Results and discussion

The CO standard gases of 10 and 200 ppm were measured in the laboratory by using the above described TDLAS system. The stability and detection limit of the system were analyzed. The linearity of the system was tested by measuring the CO standard gas at different concentrations. **Figures 10** and **11** display the measurement results of 10 and 200 ppm CO standard gases, respectively. After continuous measurements of 14 h, the average concentrations are 10.57 and 200.36 ppm, and the standard variance is 0.5 and 2.1 ppm, which can be found in **Table 2**. The standard variance reflects the stability of the system to a certain extent.

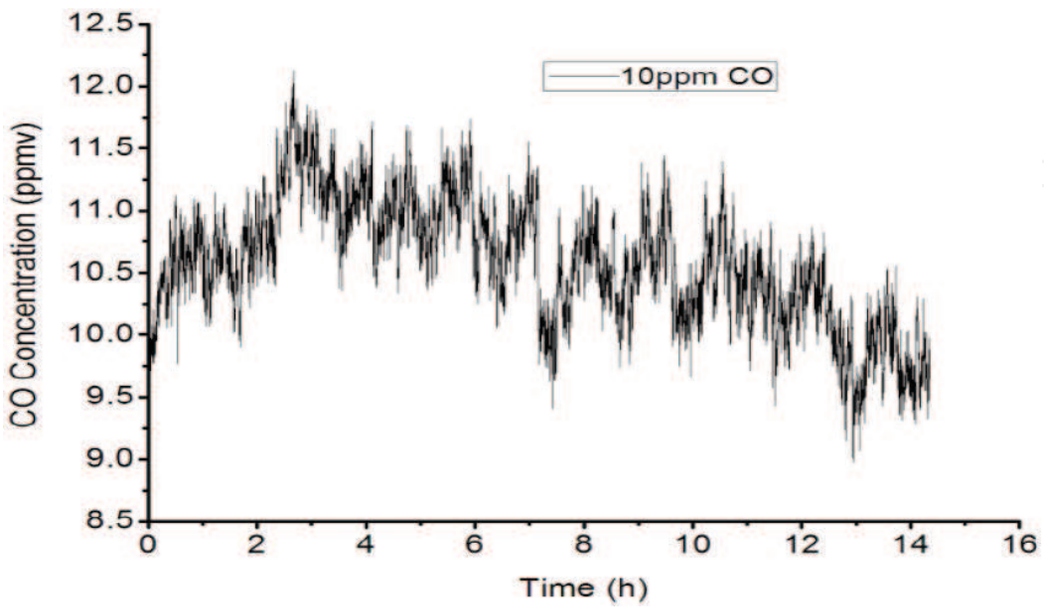

Figure 10. The measurement results of 10 ppm CO standard gas.

http://dx.doi.org/10.5772/intechopen.72948

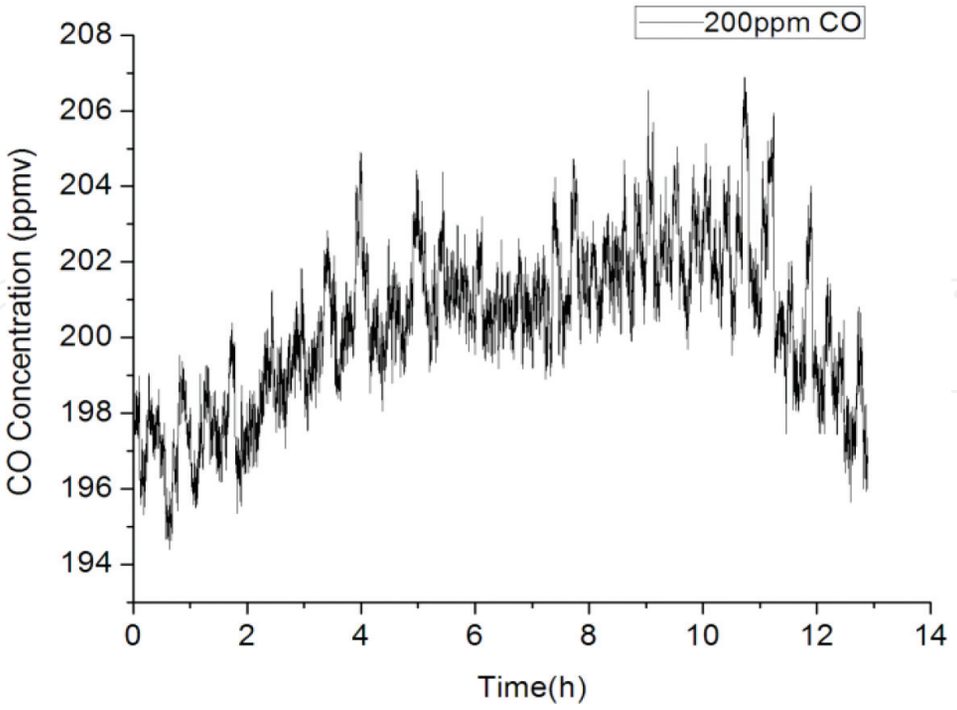

Figure 11. The measurement results of 200 ppm CO standard gas.

CO standard gas (ppm)	Mean value (ppm)	Standard deviation (ppm)	Fluctuation (%)
10	10.57	0.5	4.7
200	200.36	2.1	1

Table 2. Measured deviation of CO standard gas.

The measured concentration fluctuations of 10 and 200 ppm CO standard gas are 4.7 and 1% of the mean value, respectively. This illustrates that different concentration ranges should be divided when measuring low concentration gas with high sensitivity, such as 0–20, 20–50, 50–100 ppm, and so on, and different ranges have different stability indexes.

The results of Allan variance analysis of 10 ppm CO sample gas are shown in **Figure 12**. The corresponding integration time of the system is 30 s, the Allan variance is 0.067, and the predicted detection limit is 0.25 ppm. Moreover, if we continue to increase the integration time until the intersection with the slope of 1/2, the Allan variance decreases to 0.02, the corresponding detection limit is 0.14 ppm, but the long integration time will affect the sensitivity of the system [54]. Therefore, the integration time should be properly controlled when the requirement of detection limit is not very high. The measurement results of CO gas at different concentrations are shown in **Figure 13**, and the linear relationship between different concentrations and the peak values of second harmonic signal is displayed in **Figure 14**. The results illuminate that the measurement concentrations have a good linearity in the range of 10–250 ppm.

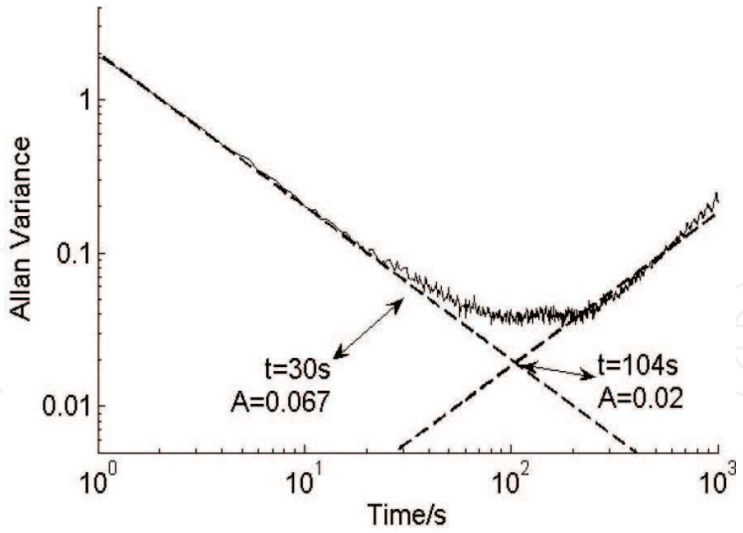

Figure 12. The Allan variance of 10 ppm CO.

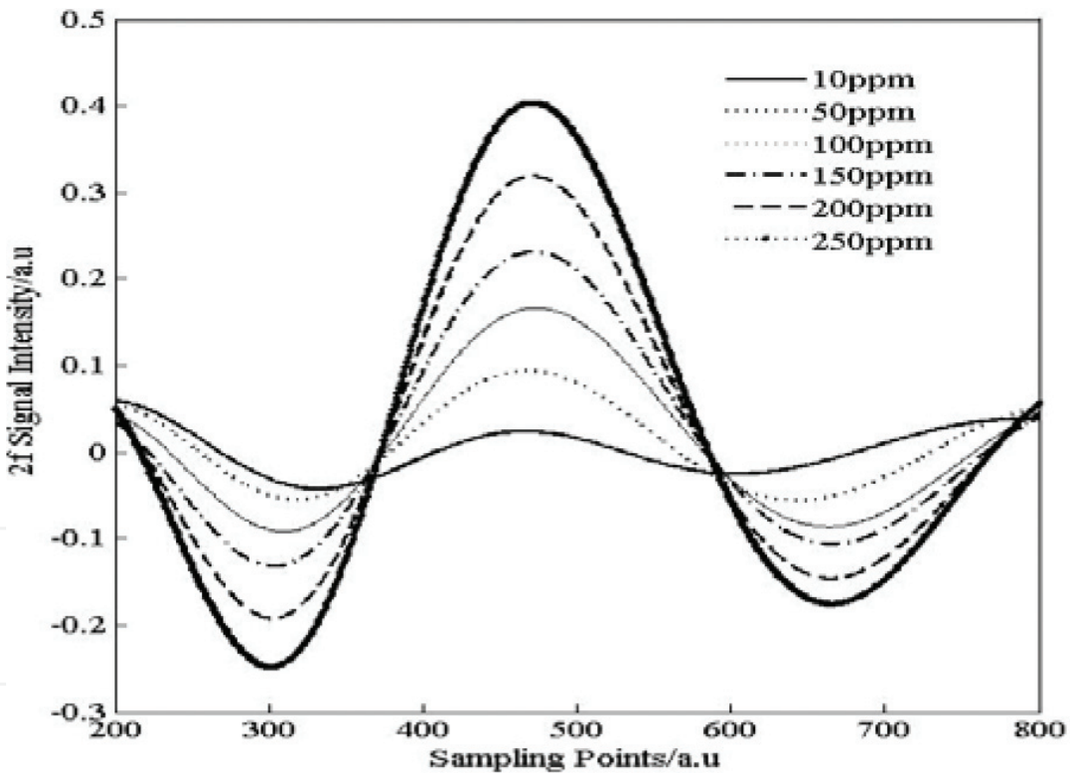

Figure 13. The 2f signals with different concentrations of CO.

The system of CO high sensitivity detection based on TDLAS technology combined with the new type of multi-pass absorption cell basically realizes the high sensitivity detection of CO in the near infrared. The system exhibits good stability and high linearity after long-term measurement experiments. According to the Allan variance analysis, the detection limit of the system is 0.25 ppm with an integration time of 30 s. The system meets the requirements for

http://dx.doi.org/10.5772/intechopen.72948

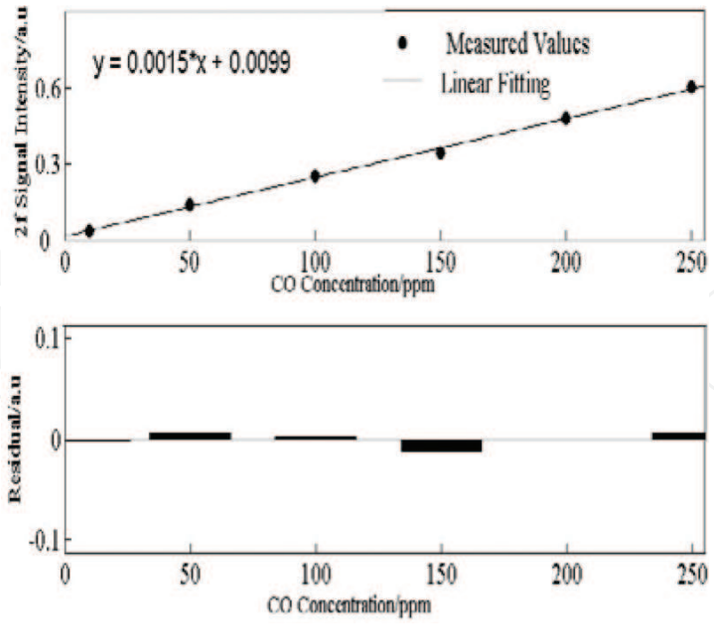

Figure 14. The linear relationship between different concentrations.

those situations which have a higher measurement requirement of CO such as alarming of coal spontaneous combustion and mine safety production. But it is only the results of experimental measurement under the laboratory conditions. For the mine environments with high temperature and humidity, the performances of the experimental relevant components need to be further tested.

5. Hydrogen sulfide (H_2S) monitoring

5.1. Introduction

Hydrogen sulfide (H_2S) is an important potential dangerous gas in oil drilling. It is colorless, highly toxic, and acidic; there is a special smell of rotten eggs; the olfactory threshold is 0.00041 ppm. Even low concentrations of H_2S can also damage people's sense of smell and have effects on the eye, respiratory system, and central nervous system. It is lethal to detect this kind of gas using a nose [55]. Because there is no smell when the concentration is high (high concentrations of hydrogen sulfide can paralyze olfactory nerves). Hence, sensitive H_2S detection is necessary in practical applications. In this part, a 1.578 μm distributed feedback (DFB) laser is used to detect H_2S of low concentration [56].

5.2. Wavelength modulation spectroscopy system

The WMS technique is used in the H_2S detection system, as shown in **Figure 15**. The used multipass absorption cell in this experiment is also homemade with a total optical path length of 56 m and a total volume of 0.8 L. A single-mode pigtailed DFB laser with a central wavelength of

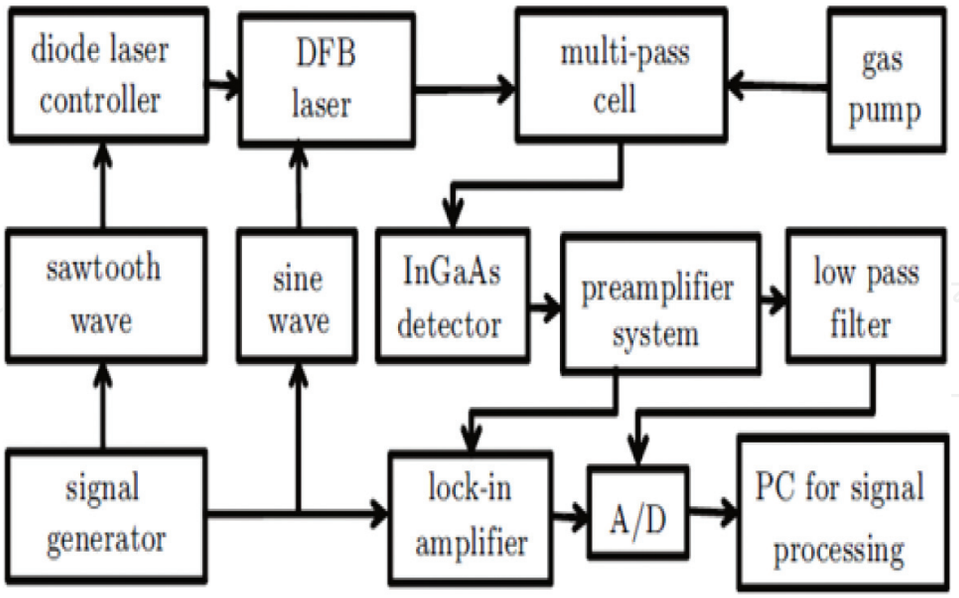

Figure 15. Sketch of the experimental setup for WMS system.

1.578 μm is employed in this system. The wavelength of the laser is controlled by a temperature and current controller, which can vary the laser wavelength with a magnitude of about 0.014 cm^{-1}/mA. The laser wavelength is scanned by a triangular wave of 30 Hz. A 20 kHz sine wave is used to modulate the laser output wavelength. The transmission signal was sent to the preamplifier system whose bias amplifier enhances the weak absorption signals. The parallel circuits amplify the signal and direct it to a lock-in amplifier for demodulation and to a low pass filter for obtaining the triangular wave after passing through the cell. Both signals are directed to a personal computer (PC) for signal processing via an A/D converter.

5.3. H_2S concentration measurements

5.3.1. Stability of the background signals

In order to improve the measurement accuracy and the detection limit, it is important to subtract the background spectrum in the spectral measurements. The background and the initial 2f signal are shown in **Figure 16**. Obviously, the symmetry of the demodulated signal was considerably improved after the background correction.

5.3.2. Linearity and response time

Linearity is an important parameter in measuring instruments. In this TDLAS system, certified H_2S gases with mixing ratios of 5, 10, 20, and 45 ppm were tested successively to check the linearity. **Figure 17** displays the corresponding background corrected signals at different mixing ratios. Furthermore, the mixing ratios and the peak-to-peak values are linearly fitted in **Figure 18**. The results illustrate that the system has a good linearity with a fitting coefficient of 0.998.

The fitting is given by y = 0.00143 + 7.52459x with a fitting coefficient of 0.998.

http://dx.doi.org/10.5772/intechopen.72948

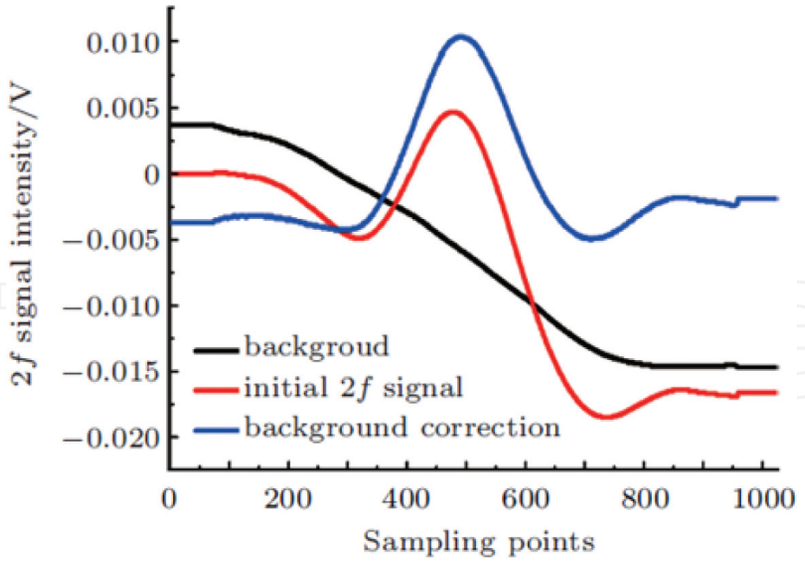

Figure 16. Background baseline.

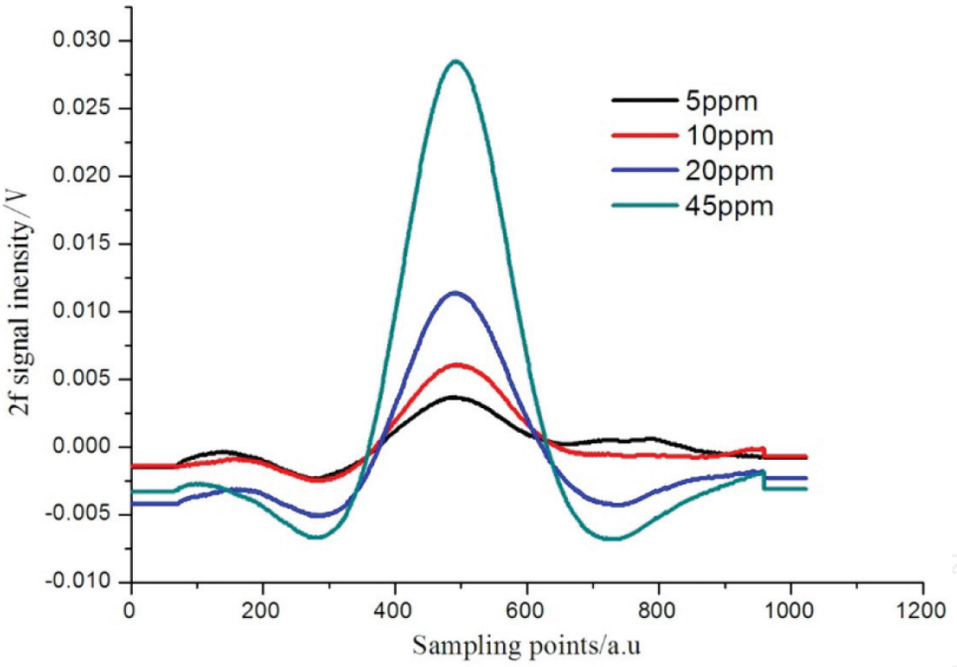

Figure 17. 2f signals with background correction for different H_2S concentrations.

The repeatability and the response time are also very important for H_2S detection. In the extraction system, a 1-L gasbag is used to get different H_2S standard gases into the multi-pass absorption cell successively. The response time depends on both the volume of the multi-pass absorption cell and the speed of releasing the airbag. The response time for filling 5 ppm H_2S standard gas mixture into the 0.8 L cell with an evacuation flow rate of 3 L/min is plotted in **Figure 19**. Obviously, the response is accurate and fast. In the system, the data sampling rate is 90 Hz, so the response time is about 4 s.

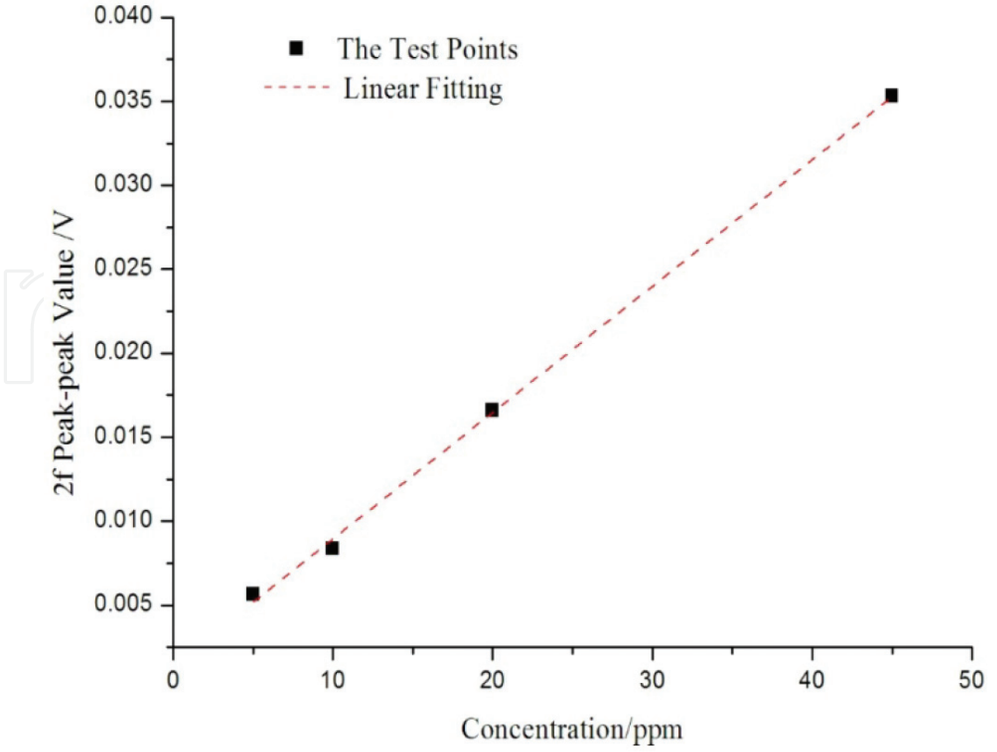

Figure 18. Linearity of the measurement system.

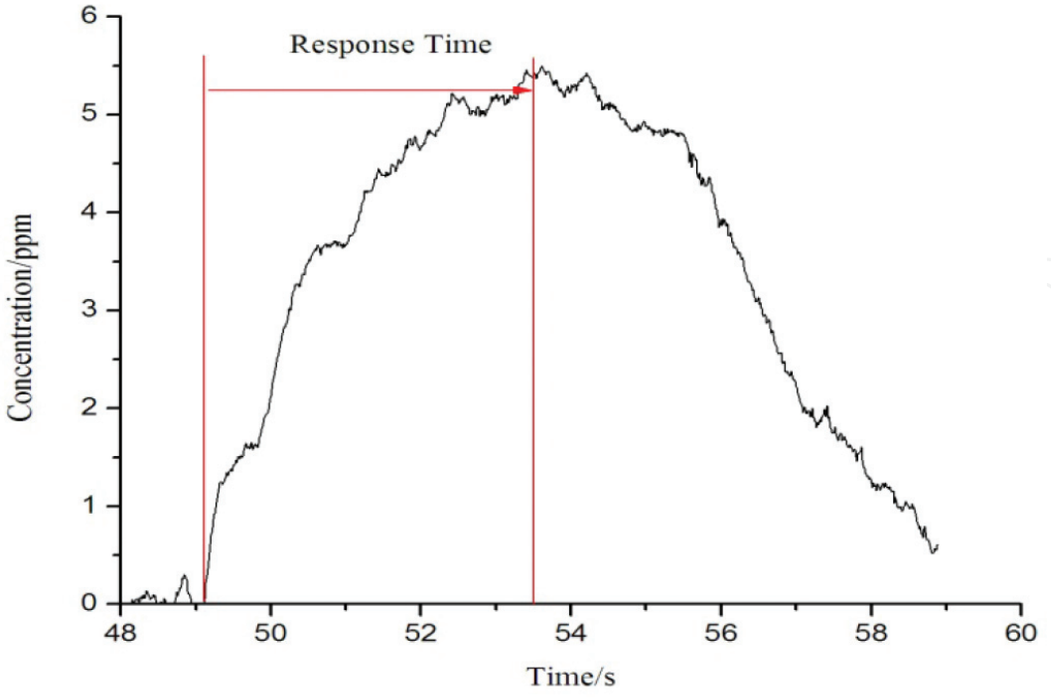

Figure 19. Response time of the measurement system.

http://dx.doi.org/10.5772/intechopen.72948

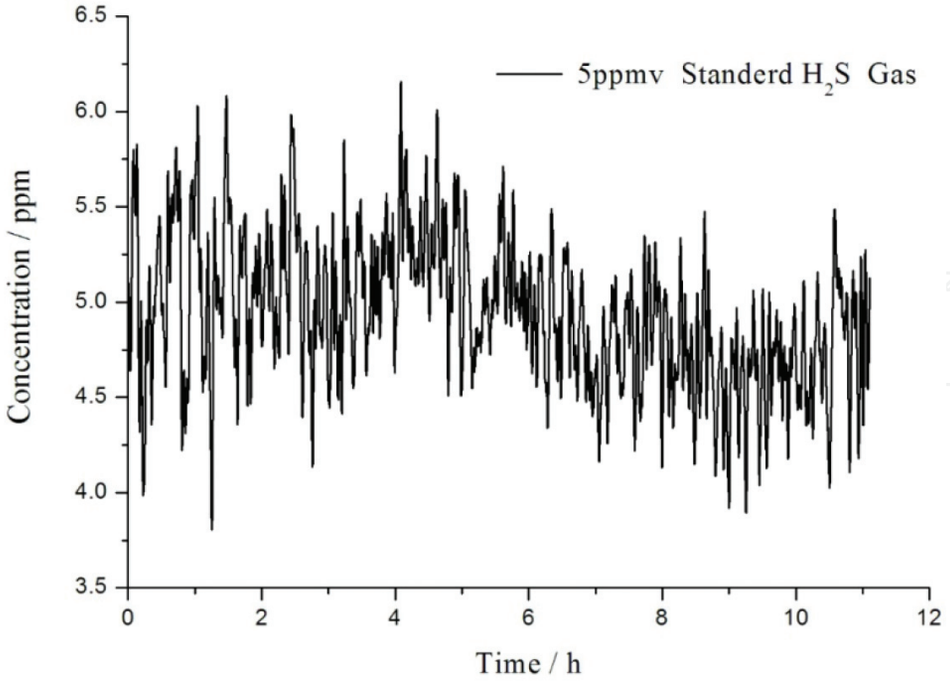

Figure 20. Measurement of 5 ppm H_2S standard gas.

5.3.3. System stability and detection limit

The Allan variance is usually used to analyze the temporal stability of the instrument performance. H_2S standard gas of 5 ppm was measured for a period time of 11 h and shown in **Figure 20** with the fluctuations of less than 1 ppm. Moreover, the Allan variance in **Figure 21** indicates a detection limit of 240 ppb with an integration time of 24 s for eliminating the white noise. When the time is increased to 60 s, the detection limit is reduced to 140 ppb for removing the 1/f noise.

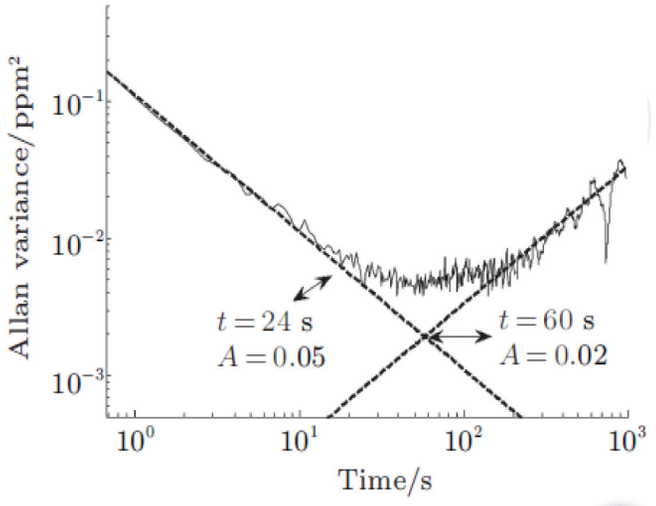

Figure 21. The Allan variance for 5 ppm H_2S.

The experimental results indicate that the system has good linearity, stability, and repeatability, combined with a quick response time and a low detection limit. The H_2S detection system based on TDLAS has the feasibility of online monitoring in many applications.

6. CO_2 isotope measurements

6.1. Introduction

Global warming is a serious problem that may lead to natural disasters, destroys the biological chain, and thus threats the existence and development of human beings. As one of the most important greenhouse gases, releasing of carbon dioxide must be controlled. Measuring and analyzing stable isotopes of atmospheric carbon dioxide are very useful to search sources and sinks of carbon dioxide in this area and seek the processes which are caused by human's activities. Moreover, human enzyme activities assessment, organ functions, and transport processes in the medical area could be achieved by noninvasive ^{13}C-breath analysis. For example, possible *Helicobacter pylori* infection of the stomach or the duodenum can be detected via ^{13}C-breath analysis. Thus ^{13}C-breath test can be easily performed and have a high patient acceptance [57].

The primary technology for determination isotopic ratio is isotope ratio mass spectrometry (IRMS) with a measurement precision from 0.01 to 0.1‰ by testing the mass of each isotope of samples. Although this method has high precision, the disadvantages of IRMS are obvious. For example, the instrument of IRMS is too large to move easily, and the sample must be pre-treated in the case of the influence of other substances whose numbers of molecules are same with those need to be tested. These drawbacks make it impossible to measure the isotopic ratio in situ or online. TDLAS is a popular way to measure concentrations of gases. According to direct absorption, concentration and isotope ratio can be easily calculated when temperature, pressure, optical path length, and absorption line strength of gases are certain.

6.2. Experimental setup

The experimental setup is depicted in **Figure 22**. The laser source is a room temperature operated DFB laser (nanoplus GmbH) with a center wavelength of 2.74 μm and a tuning range of 5 cm^{-1}. A visible He-Ne laser beam was used to do coalignment of the optical path since the mid-infrared light is not visible to human eyes. Positions of water vapor absorption lines from the HITRAN 2008 database provided an absolute frequency reference for frequency calibration. The laser beam was directed to a homemade multi-pass absorption cell with an optical path length of 107 m. In order to avoid the absorption line intensity fluctuation caused by the absorption cell temperature variation, the temperature of the multi-pass absorption cell was maintained at 30°C by the use of a heater band and a temperature controller. The emerging absorption signal from the cell was focused onto a thermoelectrically cooled (TEC) photovoltaic VIGO detector (PVI-4TE-3). The detector output was sampled with a fast data acquisition card and then transferred to a personal computer for further data processing.

http://dx.doi.org/10.5772/intechopen.72948

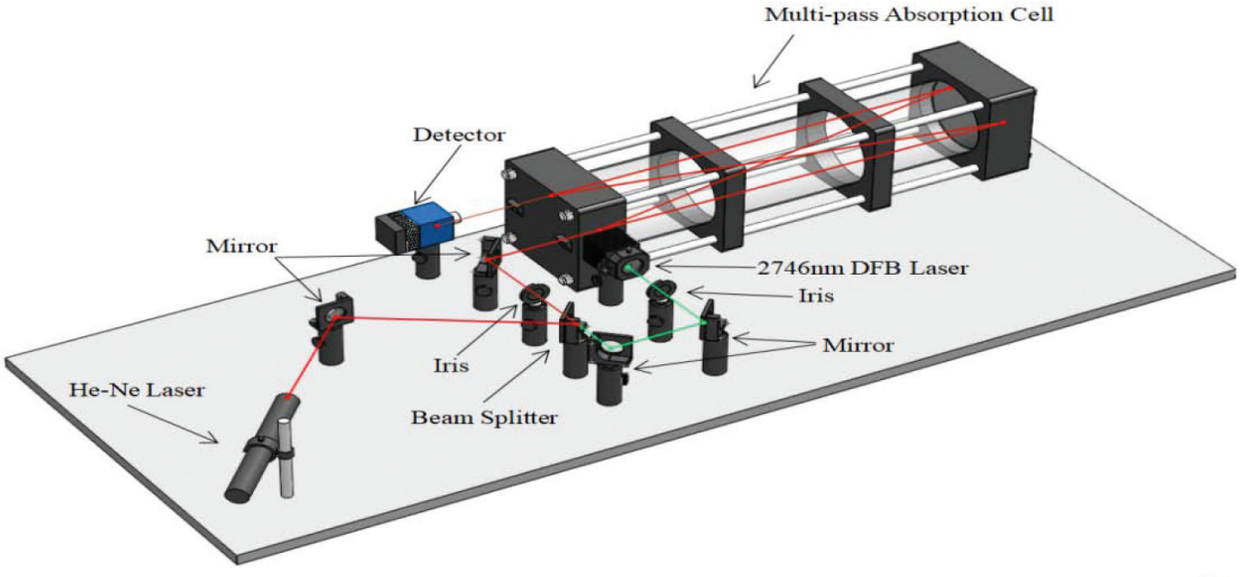

Figure 22. Three-dimensional view of the experimental setup.

6.3. Absorption line selection

For high-precision isotopic-ratio determination, it is necessary to select absorption lines which simultaneously fulfill the following conditions: (1) they should be located within the scanning range of the laser; (2) there should be no interferences from other atmospheric species, primarily water vapor; (3) the isotopologues of interest should have similar absorption strength to obtain an optimal SNR [58, 59].

Using the above requirements, it is rather straightforward to identify spectral regions that may contain suitable sets of isotopic absorption lines. Spectra simulation of 5% H_2O and 500 ppm CO_2 based on line positions and line strengths reported in the HITRAN 2008 database in the spectral range of the DFB laser scanned is displayed in **Figure 23**. The two absorption lines of

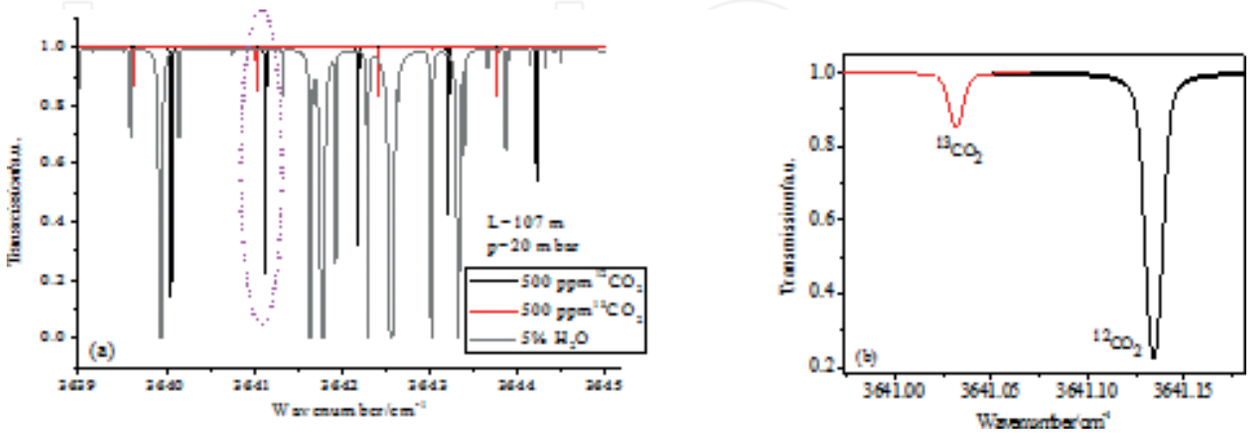

Figure 23. (a) Simulated absorption spectrum of 5% H_2O and 500 ppm CO_2 in the spectral range of 3639–3645 cm^{-1}. (b) Signal simulation of 500 ppm $^{12}CO_2$ and $^{13}CO_2$ based on HITRAN 2008 database with a path length of 107 m at a pressure of 20 mbar. $^{12}CO_2$, $^{13}CO_2$, and H_2O absorption lines are shown in black, red, and gray, respectively.

3641.0311 cm^{-1} for $^{13}CO_2$ and 3641.1338 cm^{-1} for $^{12}CO_2$ were selected for isotope analysis of CO_2 and free of interferences of water vapor absorption lines.

6.4. Results and discussion

Figure 24 shows an experimental spectrum of $^{12}CO_2$ and $^{13}CO_2$ in ambient air at 20 mbar with an optical path length of 107 m within a narrow scanned range of 0.1 cm^{-1}. Spectroscopic parameters of the selected absorption lines are provided in **Table 3**.

The instrument performance in terms of detection limit and long-term stability was tested using the Allan variance. The mixing ratios of CO_2 were measured with 1 s collection time from a standard gas cylinder with 197 ppm CO_2. Time series of this data is shown in **Figure 25**. From the associated Allan variance plot, an optimum averaging time of 130 s can be derived.

This instrument was used to measure the isotope ratios of CO_2 in the ambient air. Time series of CO_2 mixing ratio profiles and the derived $\delta^{13}C$ values with 1 s average time are shown in **Figure 26**. The measured mean value of CO_2 mixing ratios and $\delta^{13}C$ is 454 ppm and −98.75‰, respectively. The 1σ standard deviation of $\delta^{13}C$ is 1.8‰. According to the Allan variance, the optimum integration time is 130 s; the corresponding measurement precision can reach to

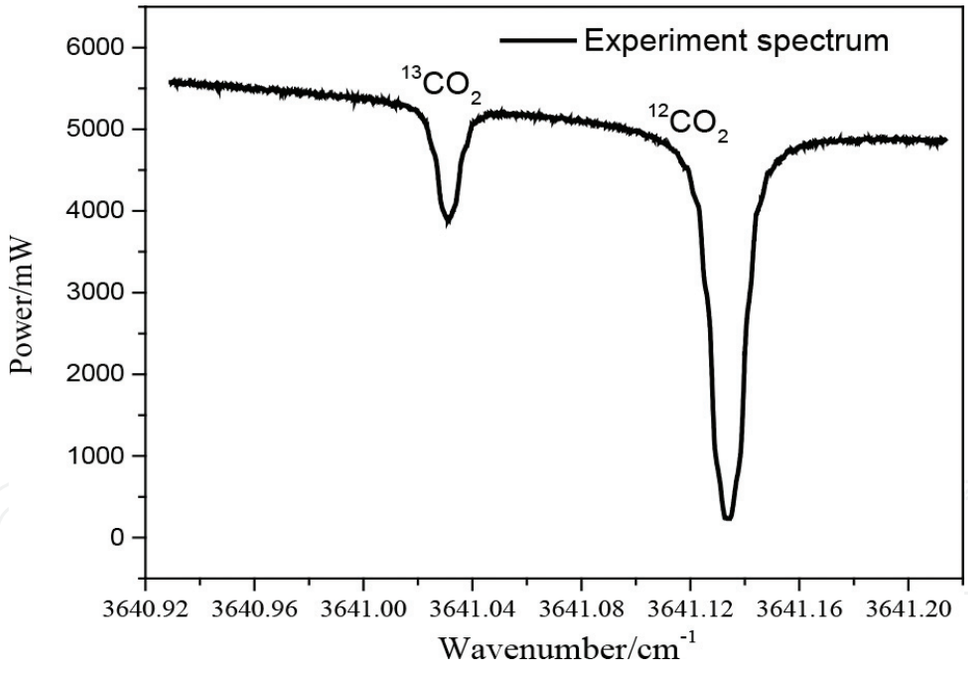

Figure 24. Direct absorption signals of $^{12}CO_2$ and $^{13}CO_2$ in ambient air at 20 mbar with an optical path length of 107 m.

Isotopologue	Wavenumber (cm^{-1})	Line strength (10^{-21} cm^{-1} cm^2/molecule)
$^{16}O^{12}C^{16}O$	3641.1338	5.637
$^{16}O^{13}C^{16}O$	3641.0311	0.641

Table 3. Spectroscopic parameters of the selected absorption lines for this work.

http://dx.doi.org/10.5772/intechopen.72948

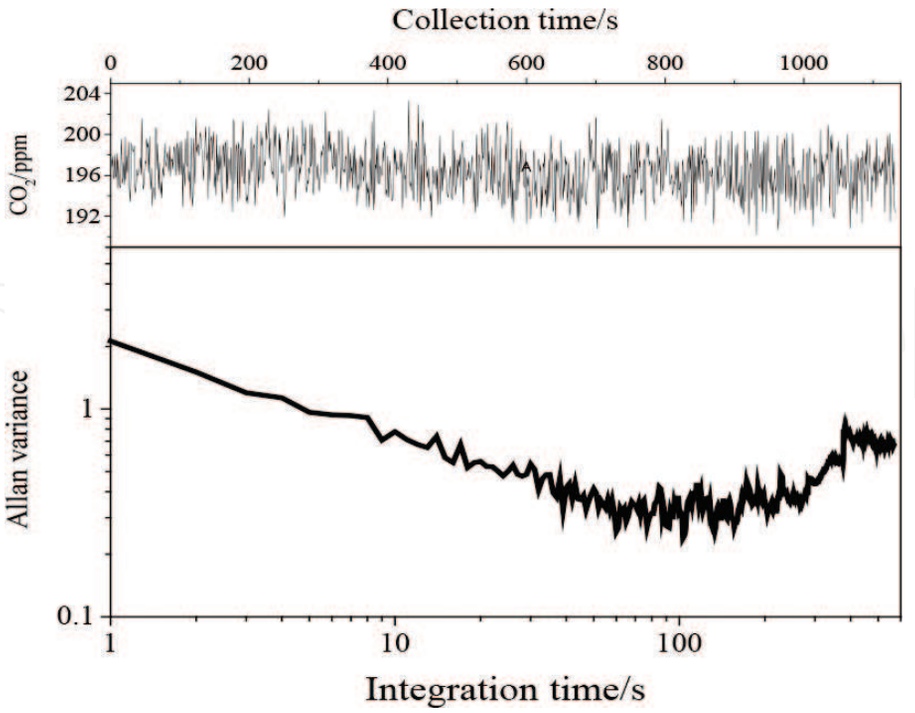

Figure 25. Time series and Allan plot of CO_2 from a standard gas cylinder.

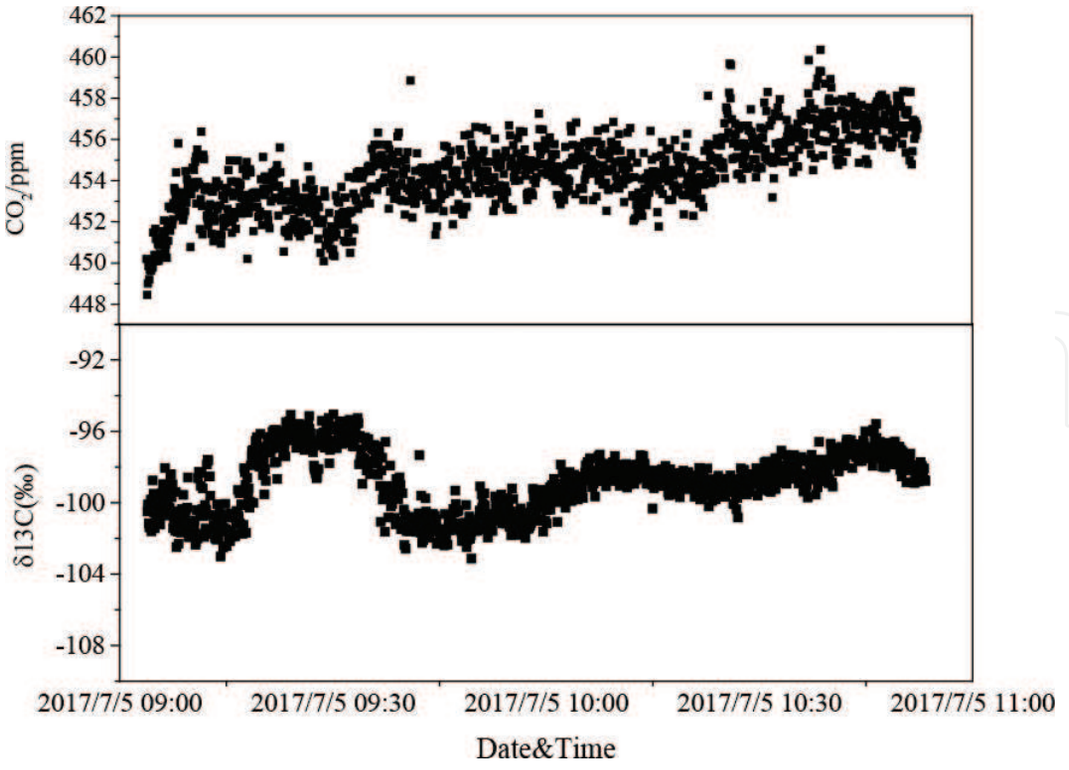

Figure 26. Time series of CO_2 mixing ratios and $\delta^{13}C$ measured by the DFB spectrometer.

0.2‰. For our CO_2 isotopologue measurement system based on TDLAS, high measurement precision has been obtained; the next step is to further improve the long-term stability of the system and perform calibration to get the correct isotope ratios and after that apply it to the medical area.

7. HONO measurements

7.1. Introduction

Gaseous nitrous acid (HONO) is a highly reactive short-lived species playing a significant role in tropospheric photochemistry. The photolysis of HONO in the wavelength range of 300–400 nm is an important source of the primary hydroxyl free radical (OH) in the lower atmosphere, up to 80% of the integrated source strength [60, 61]:

$$\mathrm{HONO} + h\nu\ (300\ \mathrm{nm} < \lambda < 400\ \mathrm{nm}) \rightarrow \mathrm{OH} + \mathrm{NO} \tag{8}$$

The OH radical governs the oxidation and removal of most pollutants from the atmosphere and is also a key species in photochemical cycles responsible for ozone formation leading to the so-called "photochemical smog" pollution. Therefore, HONO directly affects the oxidative capacity of the troposphere and indirectly contributes to production of secondary pollutants via the oxidation. Knowledge of atmospheric HONO concentration is very important for precise estimation of the OH radical budget and hence precise prediction of the impact on climate and air quality [62, 63]. In the lower atmosphere, the following formation pathways of gaseous HONO are commonly considered: (1) homogenous reaction [64, 65], (2) direct emission (i.e., by traffic) [66], and (3) heterogeneous conversion of NO_2 to HONO on the ground and other surfaces [67–71]. Homogeneous reaction and direct emissions have been identified, but these two sources are not sufficient to explain the observed atmospheric concentrations of HONO. At present, it is generally considered that HONO is mainly produced from heterogeneous process, namely, the heterogeneous reactions of NO_2 on wet surfaces as well as on surface of reducing substances such as carbon black aerosol surface [72–74]. Despite a large amount of research, the sources and the formation mechanisms of HONO in the atmosphere are still not well understood and identified due to the lack of accurate local measurements [75].

Good understanding of HONO sources and sinks requires instruments capable of performing high sensitivity, high precision, high specificity, high spatial resolution, and fast in situ measurements. Among various analytical instruments developed for field HONO monitoring [76–78], spectroscopic detection techniques capable of performing in situ measurements without any sample preparation have been increasingly developed since last decade as an attractive alternative for quantitative assessments of HONO in the atmosphere. Methods such as DOAS, incoherent broadband cavity-enhanced absorption spectroscopy (IBBCEAS), and the long-path absorption photometer (LOPAP) used in the ultraviolet region usually can get several hundred ppt-level detection limits, but the integration time of several minutes is long and cannot satisfy the requirement of fast measurements [6, 79]. In the mid-infrared region, the continuous-wave

quantum cascade lasers (cw-QCL) combined with a multi-pass absorption cell based on TDLAS technology were applied to the measurement of atmospheric HONO with a sub-ppb detection limit [80–85]. The advantages of using cw-QCLs in TDLAS over lead salt lasers are better mode stability, higher laser output power, and room temperature operation without the need for cryogenic cooling, which facilitates long-term field measurements.

7.2. QCL-based instrumental platform

The developed QCL instrumental approach is depicted in **Figure 27**. It was based on a room temperature operation cw distributed feedback (DFB) quantum cascade laser (DQ7-M776H, Maxion Technologies, Inc.). It emitted single-mode laser power of up to 35 mW. The wavelength tuning of ~2 cm^{-1} around 1254 cm^{-1} might be achieved by ramping laser injection current and/or temperature tuning. The pre-collimated laser beam from the QCL was first coupled to a beam splitter (with 90% transmission and 10% reflection). In order to make the optical alignment easy, a visible He-Ne laser beam was adjusted to be coaxial with the invisible infrared beam from the QCL. The transmitted light was directed to a multi-pass cell with a base length of 0.8 m and a folded path length of 158 m. The emerging absorption signal from the multi-pass cell was focused onto a thermoelectrically cooled (TEC) photovoltaic VIGO detector (detector 1: PVI-4TE-10.6). The reflected beam was directed to a homemade Fabry-Perot etalon with a free spectral range of 0.03 cm^{-1}. The optical fringe signal was recorded with another VIGO detector (detector 2: PVMI-10.6) and used for relative wavelength metrology. The pressure in the multi-pass cell was

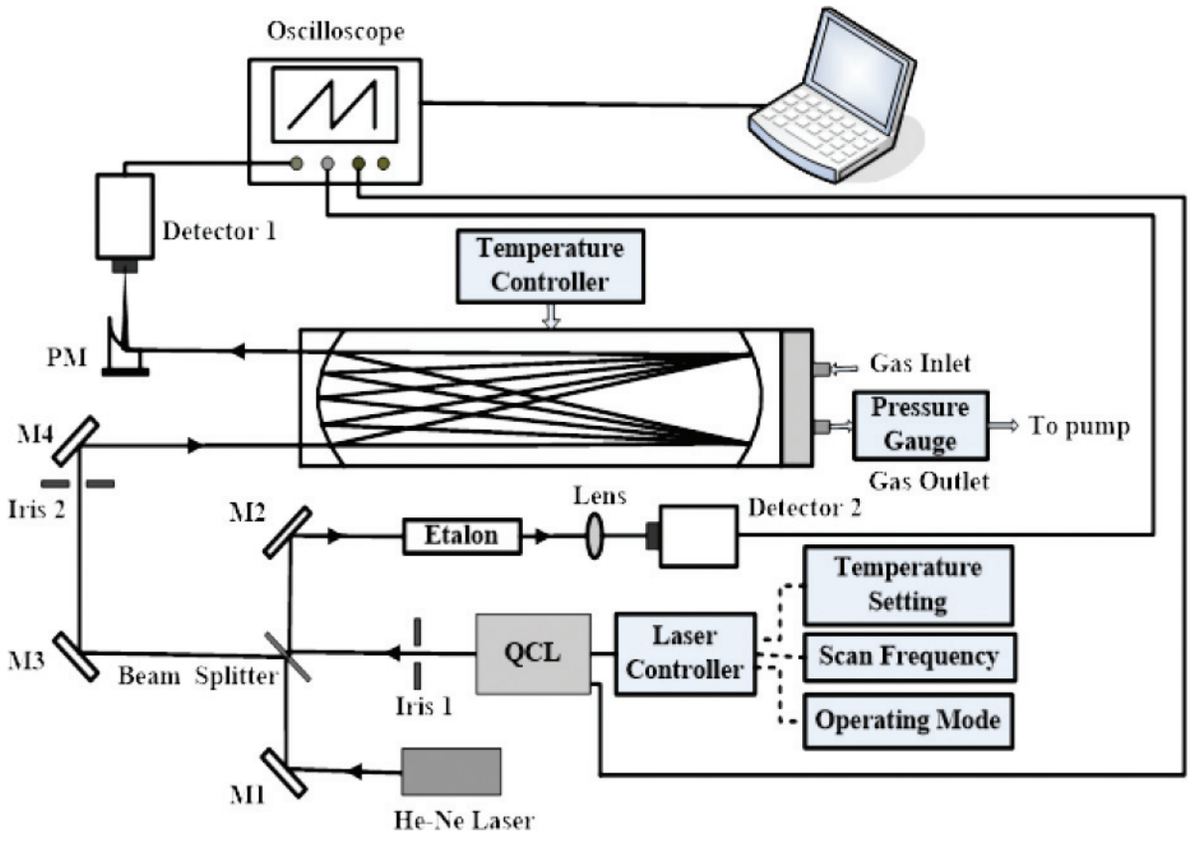

Figure 27. Schematic diagram of the experimental setup. Lens: f = 50 mm. PM (parabolic mirror): f = 25 mm. M: Mirror.

measured with a pressure transducer (Pfeiffer Vacuum, CMR 361). Temperature of the multi-pass cell was maintained at 30°C (within ±0.1°C) in order to avoid deposit of aqueous nitrous acid on the optical cell wall (especially on the cell mirrors) and to avoid any artifact production due to heterogeneous reaction inside the cell. The two detector outputs were sampled with a fast data acquisition digital oscilloscope (LeCroy Wavesurfer 104Xs-A). The data was then transferred to a personal computer for further data processing.

7.3. Results and discussion

7.3.1. Continuous monitoring of atmospheric HONO

The developed QCL instrument was employed for monitoring daytime and nighttime variation of HONO in an urban environment near a road with moderate traffic. Continuous monitoring of HONO mixing ratio variation was performed during a campaign of several days. **Figure 28** shows time series of the mixing ratios of 15 min averages of HONO and NO_2 and the corresponding ratios of $HONO/NO_2$ along with the solar radiation for the field measurements from 14 to 18 January 2013 (16–18 of them are snowy days). NO_2 was measured by a NO_x analyzer (Environmental SA). The solar radiation was recorded by a weather station (Davis Vantage Pro2, Montanay). The measured HONO mixing ratios ranged from 1.40 ppb to

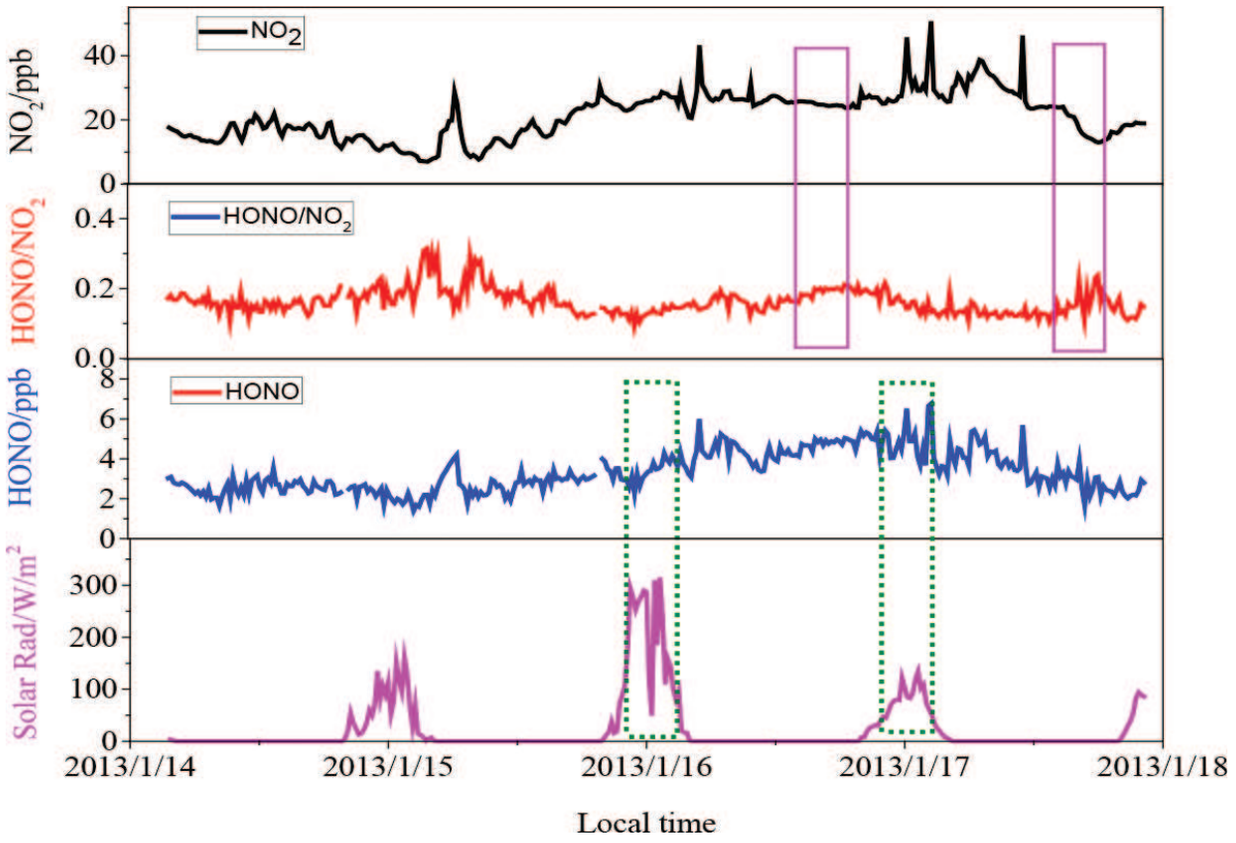

Figure 28. Time series of HONO, NO_2, the solar radiation, and $HONO/NO_2$ during the field measurements from 14 to 18 January 2013.

http://dx.doi.org/10.5772/intechopen.72948

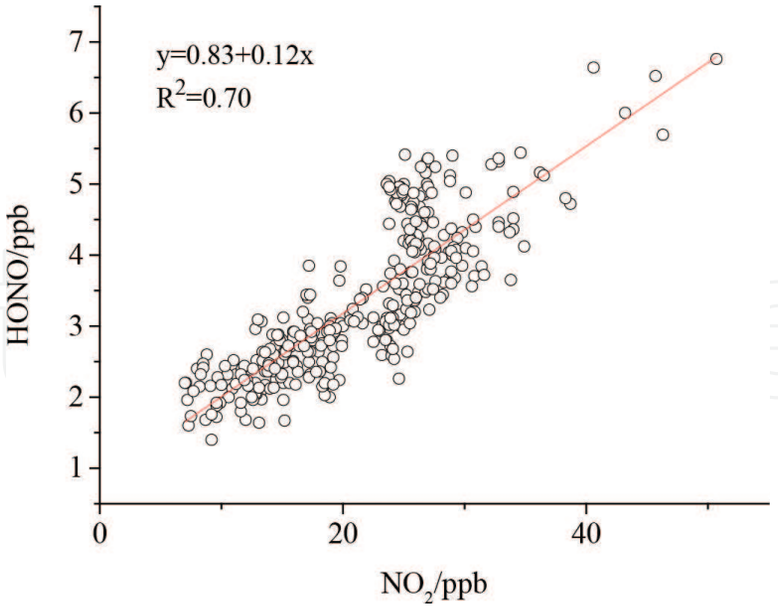

Figure 29. Correlation between HONO and NO_2 during the measurement period.

6.76 ppb, with a mean value of 3.33 ± 1.03 ppb, whereas the mean and maximum mixing ratios of NO_2 were 21.32 ± 7.36 ppb and 50.70 ppb, respectively.

7.3.2. Possible sources of HONO

NO_2 is known to be an important precursor for the formation of HONO or to have a common source. As mentioned in the introduction, the mixing ratios of HONO and NO_2 were found to be highly correlated in many field observations [77, 86]. The regression analysis (shown in **Figure 29**) of the combined data sets indicates good correlation between HONO and NO_2 mixing ratios, displaying an intercept of 0.83, slope of 0.12, and R^2 of 0.70. This slope can be interpreted as an upper limit for estimate of the HONO exhaust fraction of NO_2 emissions. The two parts marked with purple rectangles in **Figure 28** implied other sources of HONO formation, because of the increasing fraction of $HONO/NO_2$ with decreasing NO_2 mixing ratios. The higher mixing ratios of HONO in the morning are considered as products of heterogeneous reactions of NO_2 on wet surfaces during nighttime. The two green rectangles in **Figure 28** show a record of HONO mixing ratio variation with solar radiation on snow days. A photochemically enhanced HONO production from snowpack under solar radiation can be seen [73]. Finding the missing sources and the formation mechanism of HONO in the atmosphere is still the actual topic for tropospheric HONO chemistry.

8. Summary and outlook

In conclusion, we overviewed our recent developments of several gas sensors based on TDLAS technology for in situ monitoring of hazard gases, including CH_4, CO_2, CO, HONO, H_2S, and $^{13}CO_2/^{12}CO_2$. Good understanding of the sources and sinks of these hazard gases requires

instruments capable of performing high sensitivity, high precision, high specificity, high spatial resolution, and fast in situ measurements. TDLAS is an effective method to measure these gases' mixing ratios and multiple parameters with these advantages. The methane detection system based on TDLAS can simultaneously detect CH_4, C_2H_2, and C_2H_4 rapidly and effectively in open environment, and the response time is less than 2 s. The MDLs of these three gases can meet the requirements for the detection of natural gas leakage to petrochemical industry. The accuracy of making an alarm is 100%, which can be used in natural gas station and valve room gas leakage detection. The detection limit of CO detection system based on TDLAS technology is 0.25 ppm with an integration time of 30 s, which basically realizes the high sensitivity detection of CO in the near infrared and satisfies the requirements for those situation that have a higher measurement requirement of CO such as alarming of coal spontaneous combustion and mine safety production. The experimental results of H_2S show that the system based on TDLAS has a good linearity and stability with a quick response time of 24 s and a low detection limit of 240 ppb. This indicates that the system has the feasibility of real-time online monitoring in many applications. The measurement system of CO_2 isotopologues has realized the high measurement precision of 0.2‰ for $\delta^{13}C$; the next step is to carry out calibration to get the correct isotope ratios and achieve long-term stability measurements. Good understanding of the important roles of HONO in the key chemical processes of hydroxyl radicals and the sources of HONO requires correct detection of the HONO mixing ratios. A QCL-based instrumental system was designed to measure the atmospheric HONO. The regression analysis indicates good correlation between HONO and NO_2. But increasing HONO mixing ratios with decreasing NO_2 also indicates other sources of HONO formation. Finding the missing sources and the formation mechanism of HONO in the atmosphere is still a great challenge for tropospheric HONO chemistry.

Although parts of these gas analysis experiments are just results under laboratory conditions, we are improving the stability and SNR of these systems with the aim of putting them into practical application. To date we have developed all-fiber gas sensor to detect CH_4, O_2, C_2H_2, and C_2H_4, portable CH_4 sensors, CO_2 analyzer, CO analyzer, and so on. Some of them have been put into the application. The development of these gas sensors would be beneficial for the implementation of environmental protection policies and expand their application in energy, public safety, and medical science. The TDLAS technology also shows high potential for monitoring all kinds of hazardous gases in the atmosphere from surface layer to troposphere combined with a wide spectral application range from the near infrared to mid-infrared.

Acknowledgements

This work is partly supported by National Natural Science Foundation of China (Grant No. 41775128, 41405034, 11204319), the External Cooperation Program of the Chinese Academy of Sciences (Grant No. GJHZ1726), the Special Fund for Basic Research on Scientific Instruments of the Chinese Academy of Science (Grant No. YZ201315), and the Chinese Academy of Science President's International Fellowship Initiative (PIFI, 2015VMA007). Finally, the Scientific Research Foundation for the Returned Overseas Chinese Scholars, State Education Ministry, is gratefully acknowledged.

Author details

Xiaojuan Cui[1,2], Fengzhong Dong[1,2,3]*, Zhirong Zhang[1,2], Hua Xia[1,2], Tao Pang[1], Pengshuai Sun[1], Bian Wu[1], Shuo Liu[1,3], Luo Han[1,3], Zhe Li[1,3] and Runqing Yu[1,3]

*Address all correspondence to: fzdong@aiofm.ac.cn

1 Anhui Provincial Key Laboratory of Photonic Devices and Materials, Anhui Institute of Optics and Fine Mechanics, Chinese Academy of Sciences, Hefei Anhui, China

2 Key Laboratory of Environmental Optics and Technology, Anhui Institute of Optics and Fine Mechanics, Chinese Academy of Sciences, Hefei, China

3 University of Science and Technology of China, Hefei, China

References

[1] Zhang Z, Pang T, Yang Y, Xia H, Cui X, Sun P, Wu B, Wang Y, Sigrist MW, Dong F. Development of a tunable diode laser absorption sensor for online monitoring of industrial gas total emissions based on optical scintillation cross-correlation technique. Optics Express. 2016;**24**(10):A943-A955. DOI: 10.1364/OE.24.00A943

[2] Dong F, Liu W, Chu Y, Li J, Zhang Z, Wang Y, Pang T, Wu B, Tu G, Xia H, Yang Y, Shen C, Wang Y, Ni Z, Liu J. Real-time in situ measurements of industrial hazardous gas concentrations and their emission gross. InTech Publisher. 2011:66-90. DOI: 10.5772/27161

[3] Nelson DD, McManus B, Urbanski S, Herndon S, Zahniser MS. High precision measurements of atmospheric nitrous oxide and methane using thermoelectrically cooled mid-infrared quantum cascade lasers and detectors. Spectrochimica Acta A. 2004;**60**(14):3325-3335. DOI: 10.1016/j.saa.2004.01.033

[4] Wojtas J, Bielecki Z, Stacewicz T, Mikolajczyk J, Rutecka B, Medrzycki R. Nitrogen oxides optoelectronic sensors operating in infrared range of wavelengths. Acta Physica Polonica. 2013;**124**(124):592-594. DOI: 10.12693/APhysPolA.124.592

[5] Vardag SN, Hammer S, O'Doherty S, Spain TG, Wastine B, Jordan A, Levin I. Comparisons of continuous atmospheric CH_4, CO_2 and N_2O measurements-results of InGOS travelling instrument campaign at Mace head. Atmospheric Chemistry and Physics. 2014;**14**(7):8403-8418. DOI: 10.5194/acpd-14-10429-2014

[6] Wu T, Zha Q, Chen W, Xu Z, Wang T, He X. Development and deployment of a cavity enhanced UV-LED spectrometer for measurements of atmospheric HONO and NO_2 in Hong Kong. Atmospheric Environment. 2014;**95**(1):544-551. DOI: 10.1016/j.atmosenv.2014.07.016

[7] Lima JP, Vargas H. Mikl'os a, Angelmahr M, Hess P. Photoacoustic detection of NO_2 and N_2O using quantum cascade lasers. Applied Physics B: Lasers and Optics. 2006;**85**(2):279-284. DOI: 10.1007/s00340-006-2357-0

[8] Ma Y, Lewicki R, Razeghi M, Tittel FK. QEPAS based ppb-level detection of CO and N_2O using a high power CW DFB-QCL. Optics Express. 2013;**21**(1):1008-1019. DOI: 10.1364/OE.21.001008

[9] Bjorneberg DL, Leytem AB, Westermann DT, Griffiths PR, Shao L, Pollard MJ. Measurement of atmospheric ammonia, methane, and nitrous oxide at a concentrated dairy production facility in southern Idaho using open-path FTIR spectrometry. Transactions of the ASABE. 2009;**52**(5):1749-1756. DOI: 10.13031/2013.29137

[10] Kleffmann J, Lorzer JC, Wiesen P, Kern C, Trick S, Volkamer R, Rodenas M, Wirtz K. Intercomparison of the DOAS and LOPAP techniques for the detection of nitrous acid (HONO). Atmospheric Environment. 2006;**40**(20):3640-3652. DOI: 10.1016/j.atmosenv.2006.03.027

[11] Cui X, Dong F, Sigrist MW, Zhang Z, Wu B, Xia H, Pang T, Sun P, Fertein E, Chen W. Investigation of effective line intensities of trans-HONO near 1255 cm^{-1} using continuous-wave quantum cascade laser spectrometers. Journal of Quantitative Spectroscopy and Radiation Transfer. 2016;**182**:277-285. DOI: 10.1016/j.jqsrt.2016.06.014

[12] Rocco A, Natale GD, Natale PD, Gagliardi G, Gianfrani L. A diode-laser-based spectrometer for in-situ measurements of volcanic gases. Applied Physics B: Lasers and Optics. 2004;**78**(2):235-240. DOI: 10.1007/s00340-003-1339-8

[13] D'Amato F, Mazzinghi P, Castagnoli F. Methane analyzer based on TDL's for measurements in the lower stratosphere: Design and laboratory tests. Applied Physics B: Lasers and Optics. 2002;**75**(2–3):195-202. DOI: 10.1007/s00340-002-0981-x

[14] Sauer GC, Pisano TJ, Fitz RD. Tunable diode laser absorption spectrometer measurements of ambient nitrogen dioxide, nitric acid, formaldehyde, and hydrogen peroxide in Parlier, California. Atmospheric Environment. 2003;**37**(12):1583-1591. DOI: 10.1016/S1352-2310(03)00004-9

[15] Nelson DD, Shorter JH, Mcmanus JB, Zahniser MS. Sub-part-per-billion detection of nitric oxide in air using a thermo electrically cooled mid-infrared quantum cascade laser spectrometer. Applied Physics B: Lasers and Optics. 2002;**75**(2–3):343-350. DOI: 10.1007/s00340-002-0979-4

[16] Hancock G, Kasyutich VL, Ritchie GAD. Wavelength-modulation spectroscopy using a frequency-doubled current-modulated diode laser. Applied Physics B: Lasers and Optics. 2002;**74**(6):569-575. DOI: 10.1007/s003400200863

[17] Werle PW, Mazzinghi P, Amato FD, Rosa MD, Maurer K, Slemr F. Signal processing and calibration procedures for in situ diode-laser absorption spectroscopy. Spectrochimica Acta Part A. 2004;**60**(8–9):1685-1705. DOI: 10.1016/j.saa.2003.10.013

[18] Liu X, Jeffries JB, Hanson RK, Hinckley KM, Woodmansee MA. Development of a tunable diode laser sensor for measurements of gas turbine exhaust temperature. Applied Physics B: Lasers and Optics. 2006;**82**(3):469-478. DOI: 10.1007/s00340-005-2078-9

[19] Roller C, Fried A, Walega J, Weibring P, Tittel F. Advances in hardware, system diagnostics software, and acquisition procedures for high performance airborne tunable diode laser measurements of formaldehyde. Applied Physics B: Lasers and Optics. 2006;**82**(2): 247-264. DOI: 10.1007/s00340-005-1998-8

[20] Varga A, Bozoki Z, Szakall M, Szabo G. Photoacoustic system for on-line process monitoring of hydrogen sulfide (H_2S) concentration in natural gas streams. Applied Physics B: Lasers and Optics. 2006;**85**(2–3):315-321. DOI: 10.1007/s00340-006-2388-6

[21] Werle P. Accuracy and precision of laser spectrometers for trace gas sensing in the presence of optical fringes and atmospheric turbulence. Applied Physics B: Lasers and Optics. 2011;**102**(2):313-329. DOI: 10.1007/s00340-010-4165-9

[22] Cassidy DT, Reid J. Baseline correction method for second-harmonic detection with tunable diode lasers. Applied Optics. 1982;**183**(86):141-154. DOI: 10.1016/0003-2670(86)80082-4

[23] Tanaka K, Tonokura K. Sensitive measurements of stable carbon isotopes of CO_2 with wavelength modulation spectroscopy near 2 μm. Applied Physics B: Lasers and Optics. 2011;**105**(2):463-469. DOI: 10.1007/s00340-011-4666-1

[24] Sappev AD, Masterson P, Huelson E, Howell J, Estes M, Hofvander H, Jobson A. Results of closed-loop coal-fired boiler operation using a TDLAS sensor and smart process control software. Combustion Science and Technology. 2011;**183**(11):1282-1295. DOI: 10.1080/00102202.2011.590560

[25] Zhang Z, Xia H, Dong F, Pang T, Wu B, Sun P, Wang G, Wang Y. Simultaneous detection of multiple gas concentrations with multi-frequency wavelength modulation spectroscopy. Europhysics Letters. 2013;**104**(4), 44002. DOI: 10.1209/0295-5075/104/44002

[26] Witzel O, Klein A, Meffert C, Wagner S, Kaiser S, Schulz C, Ebert V. VCSEL-based, high-speed, in situ TDLAS for in-cylinder water vapor measurements in IC engines. Optics Express. 2013;**21**(17):19951-19965. DOI: 10.1364/OE.21.019951

[27] Liu C, Xu L, Chen J, Cao Z, Lin Y, Cai W. Development of a fan-beam TDLAS-based tomographic sensor for rapid imaging of temperature and gas concentration. Optics Express. 2015;**23**(17):22494-22511. DOI: 10.1364/OE.23.022494

[28] Cassidy DT, Reid J. Atmospheric pressure monitoring of trace gases using tunable diode lasers. Applied Optics. 1982;**21**(7):1185-1190. DOI: 10.1364/AO.21.001185

[29] Sepulveda-Jauregui A, Martinez-Cruz K, Strohm A, Katey MWA, Thalasso F. A new method for field measurement of dissolved methane in water using infrared tunable diode laser absorption spectroscopy. Limnology and Oceanography-Methods. 2012;**10**(7):560-567. DOI: 10.4319/lom.2012.10.560

[30] Svanberg S. Gas in scattering media absorption spectroscopy-from basic studies to biomedical applications. Laser & Photonics Reviews. 2013;**7**(5):779-796. DOI: 10.4319/lom.2012.10.560

[31] Deguchi Y, Kamimoto T, Wang ZZ, Yan JJ, Liu JP, Watanabe H, Kurose R. Applications of laser diagnostics to thermal power plants and engines. Applied Thermal Engineering. 2014;**73**(2):1453-1464. DOI: 10.1016/j.applthermaleng.2014.05.063

[32] Pogány A, Klein A, Ebert V. Measurement of water vapor line strengths in the 1.4-2.7μm range by tunable diode laser absorption spectroscopy. Journal of Quantiative Spectroscopy and Radiative Transfer. 2015;**165**:108-122. DOI: 10.1016/j.jqsrt.2015.06.023

[33] Choi DW, Jeon MG, Cho GR, Kamimoto T, Deguchi Y, Doh DH. Performance improvements in temperature reconstructions of 2-D tunable diode laser absorption spectroscopy (TDLAS). Journal of Thermal Science. 2016;**25**(1):84-89. DOI: 10.1007/s11630-016-0837-z

[34] Werle P. Tunable diode laser absorption spectroscopy: Recent findings and novel approaches. Infrared Physics and Technology. 1996;**37**(1):59-66. DOI: 10.1016/1350-4495(95)00113-1

[35] Riise H, Carlisle CB, Carr LW, Cooper DE, Martinelli RU, Menna RJ. Design of an open path near infrared diode laser sensor: Application to oxygen, water and carbon monoxide. Applied Optics. 1994;**33**(30):7059-7066. DOI: 10.1364/AO.33.007059

[36] Zhang Z, Dong F, Xia H, Tu G, Wu B, Wang Y. High sensitive monitoring of carbon monoxide in industry flue gases using tunable diode lasers. Proceedings of SPIE. 2009; **7382**:73823V-1-7. DOI: 10.1117/12.836230

[37] Viciani S, Amato FD, Mazzinghi P, Castagnoli F, Toci G, Werle P. A cryogenically operated laser diode spectrometer for airborne measurement of stratospheric trace gases. Applied Physics B: Lasers and Optics. 2008;**90**(3–4):581-592. DOI: 10.1007/s00340-007-2885-2

[38] Reid J, Labrie D. Second-harmonic detection with tunable diode lasers–comparison of experiment and theory. Applied Physics B. 1981;**26**(3):203-210. DOI: 10.1007/BF00692448

[39] Cui X, Lengignon C, Wu T, Zhao W, Wysocki G, Fertein E, Coeur C, Cassez A, Croize L, Chen W, Wang Y, Zhang W, Gao X, Liu W, Zhang Y, Dong F. Photonic sensing of the atmosphere by absorption spectroscopy. Journal of Quantitative Spectroscopy and Radiation Transfer. 2012;**113**(11):1300-1316. DOI: 10.1016/j.jqsrt.2011.11.008

[40] Wang S, Li J, Che R, Wang TA. Methane gas sensor with optic Fiber based on frequency harmonic detection technique. Journal of Applied Optics. 2004;**25**(2):44-47

[41] Kan R, Liu W, Zhang Y, Liu J, Wang M, Chen D, Chen J, Cui Y. A high sensitivity spectrometer with tunable diode laser for ambient methane monitoring. Chinese Optics Letters. 2007;**5**(1):54-57

[42] Xu Y, Qian X, Liu Z. Quantitative risk analysis on the leakage of compressed natural gas pipeline. Chinese Safety Science. 2008;**18**(1):146-149

[43] Liu X, Wang L, Jin W, et al. The development of optical remote measurement for hazardous gas leakage. Infrared Technology. 2009;**31**(10):563-572

[44] Liu M, Xiang Q, Dai Z. Studies on the leakage calculation models and optimal measurement conditions of natural gas transmission pipe line systems. Chemical Engineering of Oil and Gas. 2002;**31**(1):47-51

[45] Durry G, Li JS, Vinogradov I, Titov A, Joly L, Cousin J, Decarpenterie T, Amarouche N, Liu X, Parvitte B, Korablev O, Gerasimov M, Zéninari V. Near infrared diode laser spectroscopy of C_2H_2, H_2O, CO_2 and their isotopologues and the application to TDLAS, a tunable diode laser spectrometer for the martian PHOBOS-GRUNT space mission. Applied Physics B: Lasers and Optics. 2010;**99**(1):339-351. DOI: 10.1007/s00340-010-3924-y

[46] Nikiforova OY, Kapitanov V, Ponomarev YN. Influence of ethylene spectral lines on methane concentration measurements with a diode laser methane sensor in the 1.65 μm region. Applied Physics B: Lasers and Optics. 2008;**90**(2):263-268. DOI: 10.1007/s00340-007-2919-9

[47] Sun P, Zhang Z, Li J, Xia H, Han L, Li Z, Tan D, Ma Y, Dong F. Research on natural gas leakage monitoring technology based on the open-path measurement technique of methane. Optics Optoelectronics Technology. 2016;**14**(5):63-67

[48] Xia H, Wu B, Zhang Z, Pang T, Dong F, Wang Y. Stability study on high sensitive CO monitoring in near-infrared. Acta Physica Sinica. 2013;**62**(21):214208-1-7. DOI: 10.7498/aps.62.214208

[49] Curl RF, Tittel FK. Tunable infrared laser spectroscopy. Annual Reports Progress Chemical Section C. 2002;**98**(4050):217-270. DOI: 10.1039/b111194a

[50] Li JY, Du ZH, Ma YW, Xu KX. Dynamic thermal modeling and parameter identification for monolithic laser diode module. Chinese Physics B. 2013;**22**(3):317-322. DOI: 10.1088/1674-1056/22/3/034203

[51] Che L, Ding YJ, Peng ZM, Li XH. Calibration-free wavelength modulation spectroscopy for gas concentration measurements under low-absorbance conditions. Chinese Physics B. 2012;**21**(12):463-470. DOI: 10.1088/1674-1056/21/12/127803

[52] Rothman LS, Gamache RR, Goldman A, Brown LR, Toth RA, Pickett HM, Poynter RL, Flaud JM, Camy-Peyret C, Barbe A, Husson N, Rinsland CP, MAH S. The HITRAN database: 1986 edition. Applied Optics. 1987;**26**(19):4058-4097. DOI: 10.1364/AO.26.004058

[53] Tu G, Dong F, Wang Y, Culshaw B, Zhang Z, Pang T, Xia H, Wu B. Analysis of random noise and long-term drift for tunable diode laser absorption spectroscopy system at atmospheric pressure. IEEE Sensors Journal. 2015;**15**(6):3535-3541. DOI: 10.1109/JSEN.2015.2393861

[54] Werle P, Mucke R, Slemr F. The limits of signal averaging in atmospheric trace-gas monitoring by tunable diode-laser absorption spectroscopy (TDLAS). Applied Physics B: Lasers and Optics. 1993;**57**(2):131-139. DOI: 10.1007/BF00425997

[55] Chen WD, Kostere A, Tittel FK, Gao XM, Zhao WX. H_2S trace concentration measurements using off-axis integrated cavity output spectroscopy in the near-infrared. Applied Physics B: Lasers and Optics. 2008;**90**(2):311-315. DOI: 10.1007/s00340-007-2858-5

[56] Xia H, Dong F, Wu B, Zhang Z, Pang T, Sun P, Cui X, Han L, Wang Y. Sensitive absorption measurements of hydrogen sulfide at 1.578 μm using wavelength modulation spectroscopy. Chinese Physics B. 2015;**24**(3):180-184. DOI: 10.1088/1674-1056/24/3/034204

[57] Hofstetter D, Francesco JD, Hvozdara L, Herzig HP, Beck M. CO_2 isotope sensor using a broadband infrared source, a spectrally narrow 4.4 μm quantum cascade detector, and a Fourier spectrometer. Applied Physics B: Lasers and Optics. 2011;**103**(4):967-970. DOI: 10.1007/s00340-011-4532-1

[58] Tuzson B, Zeeman MJ, Zahniser MS, Emmenegger L. Quantum cascade laser based spectrometer for in situ stable carbon dioxide isotope measurements. Infrared Physics Technology. 2008;**51**(3):198-206. DOI: 10.1016/j.infrared.2007.05.006

[59] Tanaka K, Kojima R, Takahashi K, Tonokura K. Continuous measurements of stable carbon isotopes in CO_2 with a near-IR laser absorption spectrometer. Infrared Physics Technology. 2013;**60**(5):281-287. DOI: 10.1016/j.infrared.2013.05.011

[60] Stemmer K, Ammann M, Donders C, Kleffmannm J, George C. Photosensitized reduction of nitrogen dioxide on humic acid as a source of nitrous acid. Nature. 2006;**440**(7081):195-198. DOI: 10.1038/nature0460

[61] Li X, Rohrer F, Hofzumahaus A, Brauers T, Häseler R, Bohn B, Broch B, Fuchs H, Gomm S, Holland F, Jäger J, Kaiser J, Keutsch FN, Lohse I, Tillmann R, Wegener R, Wolfe GM, Mentel TF, Kiendler-Scharr A, Wahner A. Missing gas-phase source of HONO inferred from zeppelin measurements in the troposphere. Science. 2014;**344**(6181):292-296. DOI: 10.1126/science.aaa3777

[62] Alicke B, Geyer A, Hofzumahaus A, Holland F, Konrad S, Patz HW, Schafer J, Stutz J, Volz-Thomas A, Platt U. OH formation by HONO photolysis during the BERLIOZ experiment. Journal of Geophysical Research. 2003;**108**(D4):8247-8264. DOI: 10.1029/2001JD000579

[63] Acker K, Moller D, Wieprecht W, Meixner FX, Bohn B, Gilge S, Plass-Dulmer C, Berresheim H. Strong daytime production of OH from HNO_2 at a rural mountain site. Journal of Geophysics Letters. 2006;**33**(2). DOI: L02809, 10.1029/2005GL024643

[64] Pagsberg P, Bjergbakke E, Ratajczak E, Sillesen A. Kinetics of the gas phase reaction OH + NO (+M) → HONO (+M) and the determination of the UV absorption cross sections of HONO. Chemical Physics Letters. 1997;**272**(5–6):383-390. DOI: 10.1016/S0009-2614(97)00576-9

[65] Djehiche M, Tomas A, Fittschen C, Coddeville P. First direct detection of HONO in the reaction of Methylnitrite (CH_3ONO) with OH radicals. Environmental Science & Technology. 2010;**45**(2):608-614. DOI: 10.1021/es103076e

[66] Febo A, Perrino C. Measurement of high concentration of nitrous acid inside automobiles. Atmospheric Environment. 1995;**29**(29):345-351. DOI: 10.1016/1352-2310(94)00260-R

[67] Heikes BG, Thompson AM. Effects of heterogeneous processes on NO_3, HONO, and HNO_3 in the troposphere. Journal of Geophysical Research. 1983;**88**(C15):10883-10895. DOI: 10.1029/JC088iC15p10883

[68] Wong KW, Oh HJ, Lefer BL, Rappengluck B, Stutz J. Vertical profiles of nitrous acid in the nocturnal urban atmosphere of Houston, TX. Atmospheric Chemistry and Physics. 2011; **11**(8):3595-3609. DOI: 10.5194/acp-11-3595-2011

[69] Costabile F, Amoroso A, Wang F. Sub-mm particle size distributions in a suburban Mediterranean area. Aerosol populations and their possible relationship with HONO mixing ratios. Atmospheric Environment. 2010;**44**(39):5258-5268. DOI: 10.1016/j.atmosenv.2010.08.018

[70] Kleffmann J, Wiesen P. Heterogeneous conversion of NO_2 and NO on HNO_3 treated soot surfaces: atmospheric implications. Atmospheric Chemistry and Physics. 2005;**5**(1):77-83. DOI: 10.5194/acp-5-77-2005

[71] Stemmler K, Ammann M, Donders C, Kleffmann J, George C. Photosensitized reduction of nitroged dioxide on humic acid as a source of nitrous acid. Nature. 2006;**440**(7081):195-198. DOI: 10.1038/nature04603

[72] Ziemba LD, Dibb JE, Griffin RJ, Anderson CH, Whitlo SI, Lefer BL, Rappengluck B, Flynn J. Heterogeneous conversion of nitric acid to nitrous acid on the surface of primary organic aerosol in an urban atmosphere. Atmospheric Environment. 2010;**44**(33):4081-4089. DOI: 10.1016/j.atmosenv.2008.12.024

[73] Acker K, Mfller D, Auel R, Wieprecht W, Kalaβ D. Concentrations of nitrous acid, nitric acid, nitrite and nitrate in the gas and aerosol phase at a site in the emission zone during ESCOMPTE 2001 experiment. Atmospheric Research. 2005;**74**(1):507-524. DOI: 10.1016/j.atmosres.2004.04.009

[74] Monge ME, D'Anna B, Mazri L, Fendler AG, Ammann M, Donaldson DJ, George C. Light changes the atmospheric reactivity of soot. Proceedings of the National Academy of Sciences. 2010;**107**(15):6605-6609. DOI: 10.1073/pnas.0908341107

[75] Su H, Cheng Y, Oswald R, Behrendt T, Trebs I, Meixner FX, Andreae MO, Cheng P, Zhang Y, Pöschl U. Soil nitrite as a source of atmospheric HONO and OH radicals. Science. 2011; **333**(6039):1616-1618. DOI: 10.1126/science.1207687

[76] Wu T, Chen W, Fertein E, Cazier F, Dewaele D, Gao X. Development of an open-path incoherent broadband cavity enhanced spectroscopy based instrument for simultaneous measurement of HONO and NO_2 in ambient air. Applied Physics B: Lasers and Optics. 2012;**106**(2):501-509. DOI: 10.1007/s00340-011-4818-3

[77] Qin M, Xie P, Su H, Gu J, Peng F, Li S, Zeng L, Liu J, Liu W, Zhang Y. An observational study of the HONO–NO_2 coupling at an urban site in Guangzhou City, South China. Atmospheric Environment. 2009;**43**(36):5731-5742. DOI: 10.1016/j.atmosenv.2009.08.017

[78] Wang S, Zhou R, Zhao H, Wang Z, Chen L, Zhou B. Long-term observation of atmospheric nitrous acid (HONO) and its implication to local NO_2 levels in Shanghai, China. Atmospheric Environment. 2013;**77**(7):718-724. DOI: 10.1016/j.atmosenv.2013.05.071

[79] Gherman T, Venables DS, Vaughan S, Orphal J, Ruth AA. Incoherent broadband cavity enhanced absorption spectroscopy in the near-ultraviolet: Application to HONO and NO_2. Environmental Science & Technology. 2008;**42**(3):890-895. DOI: 10.1021/es0716913

[80] Becker K, Kleffmann J. KurtenbachR, Wiesen P. Line strength measurements of trans-HONO near 1255 cm^{-1} by tunable diode laser spectrometry. Geophysical Research Letters. 1995;**22**(18):2485-2488. DOI: 10.1029/95GL02471

[81] Schiller CL, Locquiao S, Johnson TJ, Harris GW. Atmospheric measurements of HONO by tunable diode laser absorption spectroscopy. Journal of Atomspheric Chemistry. 2001; **40**(3):275-293. DOI: 10.1023/A:1012264601306

[82] Li YQ, Schwab JJ, Demerjian KL. Fast time response measurement of gaseous nitrous acid using a tunable diode laser absorption spectrometer: HONO emission source from vehicle exhausts. Geophysical Research Letters. 2008;**35**(4):121-124. DOI: 10.1029/2007GL031218

[83] Lee BH, Wood EC, Zahniser MS, McManus JB, Nelson DD, Herndon SC, Santoni GW, Wofsy TC, Munger JW. Simultaneous measurements of atmospheric HONO and NO_2 via absorption spectroscopy using tunable mid-infrared continuous-wave quantum cascade lasers. Applied Physics B: Lasers and Optics. 2011;**102**(2):417-423. DOI: 10.1007/s00340-010-4266-5

[84] Craig IM, Taubman MS, Lea AS, Phillips MC, Josberger EE, Raschke MB. Infrared near-field spectroscopy of trace explosives using an external cavity quantum cascade laser. Optics Express. 2013;**21**(25):30401-30414. DOI: 10.1364/OE.21.030401

[85] Suter J, Bernacki B, Phillips M. Spectral and angular dependence of mid-infrared diffuse scattering from explosives residues for standoff detection using external cavity quantum cascade lasers. Applied Physics B: Lasers and Optics. 2012;**108**(4):965-974. DOI: 10.1007/s00340-012-5134-2

[86] Su H, Cheng Y, Cheng P, Zhang Y, Dong S, Zeng L, Wang X, Slanina J, Shao M, Wiedensohler A. Observation of nighttime nitrous acid (HONO) formation at a non-urban site during PRIDE-PRD2004 in China. Atmospheric Environment. 2008;**42**(25): 6219-6232. DOI: 10.1093/emboj/17.2.455